Clay minerals in late glacial and Holocene sediments of the northern and southern Aegean Sea

Werner Ehrmann [a],[*], Gerhard Schmiedl [a],[1], Yvonne Hamann [a], Tanja Kuhnt [a], Christoph Hemleben [b], Wolfgang Siebel [c]

[a] Institut für Geophysik und Geologie, Universität Leipzig, Talstrasse 35, D-04103 Leipzig, Germany
[b] Institut für Geowissenschaften, Universität Tübingen, Sigwartstrasse 10, D-72076 Tübingen, Germany
[c] Institut für Geowissenschaften, Universität Tübingen, Wilhelmstrasse 56, D-72074 Tübingen, Germany

Abstract

Different source areas, oceanography and climate regimes influenced the clay mineral assemblages and grain size distribution of two sediment cores from the North and South Aegean Sea during the last glacial and the Holocene. In the North Aegean Sea, clay mineral composition is mainly controlled by sea level evolution, melting of southeastern European glaciers, and establishment of the connection between the Black Sea and Aegean Sea. The long-term development of clay mineral assemblages in the South Aegean Sea reflects changes in the Nile discharge and African dust input. At this site, the establishment of pluvial conditions in the Nile catchment during the early to middle Holocene resulted in a substantial rise in smectite/illite ratios. In the late Holocene, stepwise aridification of the southern borderlands caused an increase in windblown sediment material and a decrease in Nile suspended material. The clay mineral records exhibit periodic millennial-scale fluctuations. In the North Aegean Sea, the changes are centred at a period of 1.3–1.8 ka and can be attributed to short-term climate and weathering changes in the northern borderlands. The changes in the South Aegean Sea are centred at periods of 3.2–4.3, 1.9–2.4 and 1.3–1.7 ka reflecting short-term changes in wind strength and Northeast African hydrology.
© 2007 Elsevier B.V. All rights reserved.

Keywords: Clay minerals; Palaeoclimate; Late Quaternary; Aegean Sea

1. Introduction

As part of the Eastern Mediterranean, the Aegean Sea is situated within a climatic transition zone. A temperate and humid climate prevails to the north and northwest and allows an ample vegetation and cultivation in southeast Europe. In contrast, arid conditions and deserts prevail on the landmasses of North Africa and the Near East (Bolle, 2003). Thus, the area is sensitive to changes in temperature, amount of rainfall, origin and pattern of storm tracks, vegetation type, and extent of deserts. The environmental changes occurring in both the low and the mid-latitudes can be documented in the sediments of the Aegean Sea. Therefore, they are particularly suitable for palaeoclimatic studies.

Although numerous high-resolution palaeoclimatic studies have been carried out on the marine record of the

* Corresponding author. Fax: +49 341 9732809.
  E-mail address: ehrmann@rz.uni-leipzig.de (W. Ehrmann).
[1] Present address: Geologisch-Paläontologisches Institut, Universität Hamburg, Bundesstrasse 55, D-20146 Hamburg, Germany.

western Mediterranean (e.g., Cacho et al., 2001, 2002; Hoogakker et al., 2004; Martrat et al., 2004), the Levantine Sea (Schilman et al., 2001), and the continental record in the Middle East (Bar-Matthews et al., 1999; Felis et al., 2004; Frumkin and Stein, 2004), only few such studies exist for the Aegean Sea (Cramp et al., 1988; Geraga et al., 2000, 2005). Most of the marine studies concentrated on faunal assemblages and the stable isotope record, but did not investigate the sedimentary record. In addition, most studies focussed on the sapropel layers and their origin (reviews of Rohling, 1994; Cramp and O'Sullivan, 1999, Meyers, 2006; Casford et al., 2002, 2003). However, comparable high-resolution sedimentological data are limited for intervals prior to and after sapropel formation.

Clay minerals are predestined as indicators of environmental changes and pathways of suspended sediments (Chamley, 1989; Weaver, 1989). The species and proportions of individual clay minerals in soils and sediments depend mainly on the climatic conditions and on the nature of the source rocks (e.g., Biscaye, 1965; Griffin et al., 1968; Windom, 1976; Petschick et al., 1996). Also in the Eastern Mediterranean Sea and the Aegean Sea, the clay mineral distribution in the surface sediments revealed different source areas and dispersal pathways reflecting the prevailing oceanic circulation and wind directions (Venkatarathnam and Ryan, 1971; Ehrmann et al., in press).

The aim of this study is to reconstruct the late glacial and Holocene environmental history in the region of the Aegean Sea by investigating temporal changes in the clay mineral assemblages and grain size composition. We present high-resolution records of the clay/silt ratio and of the main clay mineral groups smectite, illite, kaolinite and chlorite from two sites, one in the northern and one in the southern Aegean Sea. The sediment core from the northern Aegean Sea comprises the last ca. 22 ka, the core from the southern Aegean Sea the last ca. 42 ka. We mainly investigate how sediments in the Aegean Sea can be used to reconstruct (i) the long-term climate changes, (ii) the sea level rise after the Last Glacial Maximum (LGM), (iii) the discharge of the river Nile and its influence on the Aegean Sea, (iv) the influence of aeolian sediment influx from North Africa, and (v) the impact of short-term climate variability.

2. Environmental setting

The Aegean Sea is the northern part of the Eastern Mediterranean Sea and is situated between Greece and Turkey (Fig. 1). It is an essentially land-locked sea with a complex bathymetry. Broad shelf areas with a smooth morphology and a distinct shelf break at 120–140 m occur mainly along the eastern and northern Aegean Sea, much narrower shelves occur in the west (Perissoratis and Conispoliatis, 2003). Several small basins with water depths of up to 1500 m and shallow sills characterize the distal parts of the sea. The Aegean Sea is connected to the Levantine Sea and the Ionian Sea in the south through several seaways between southwest Turkey, Rhodes, Karpathos, Crete and the Peloponnesus. In the northeast it is connected to the Black Sea via the Dardanelles, the Marmara Sea and the Bosphorus.

Numerous rivers discharge into the eastern and northern Aegean Sea (Fig. 1). These rivers carry a significant suspension load into the ocean (see compilation by Ehrmann et al., in press). In the northwest and north, Pinios, Aliakmon, Axios, Strimon, Nestos and Evros/Meric are the most important rivers. They drain southeast Europe. In the east, the rivers Bakircay, Gediz, Kücük Menderes and Büyük Menderes discharge into the Aegean Sea. These rivers drain western Turkey. An additional but minor sediment influx occurs through the Dardanelles Strait, which is fed by the Marmara Sea and the Black Sea.

Prevailing northwest Etesian winds influence the Aegean Sea and the corresponding aeolian dust assemblage originates in the soils of southern Europe. However, this aeolian sediment influx is quantitatively negligible compared to the extensive sediment supply by rivers (Chester et al., 1977). Aeolian influx from the eastern borderlands of the Eastern Mediterranean Sea is also limited, because of the prevailing southeast and northeast winds. In contrast, Scirocco winds from the south transport large amounts of sediments during short events from the central and eastern parts of the North African desert into the Eastern Mediterranean Sea. In the southern part of the Eastern Mediterranean Sea, aeolian dust therefore is a significant constituent of the marine sediments (Venkatarathnam and Ryan, 1971; Pye, 1992). In the Aegean Sea, however, aeolian dust derived from the south is only a secondary contribution to the land-derived material (Chester et al., 1977; Kubilay et al., 1997).

Thus, the main sediment input is by river discharge. The coarser sediment components accumulate on the broad shelf areas and build up deltas. The finer sediment fraction is transported further offshore and may be distributed by ocean currents. The typical surface sediments of the Aegean basin are muds with variable proportions of calcareous planktic and benthic nano- and microfossils (Aksu et al., 1995; Geraga et al., 2005). Within the Quaternary sediment sequence, a few tephra layers occur and document the volcanic activity in the
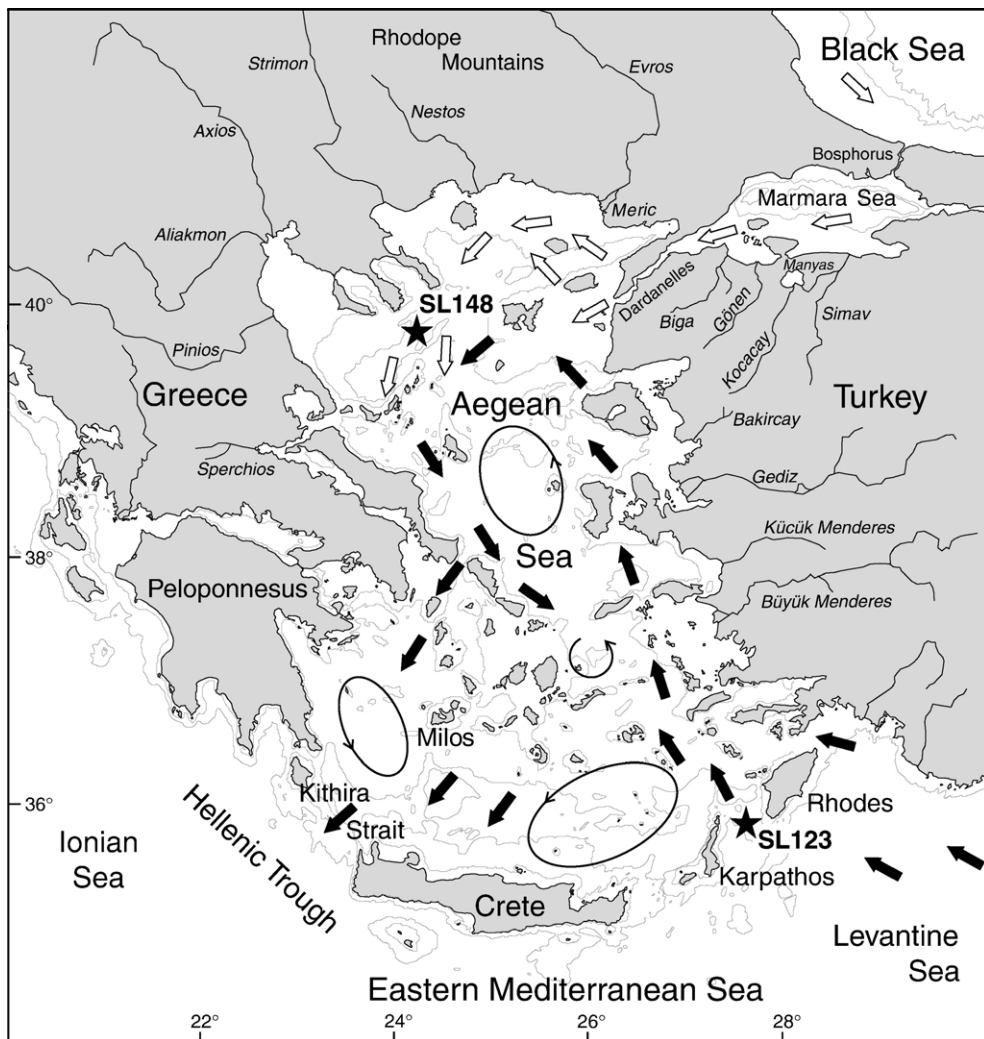
Fig. 1. Location map of the Aegean Sea with the positions of the investigated cores GeoTü SL148 and GeoTü SL123. Surface circulation follows Aksu et al. (1995) and Lykousis et al. (2002): Light arrows indicate low salinity Black Sea water, black arrows indicate warm and high salinity Mediterranean Sea water. 200 m and 1000 m depth contours are given.

southern part of the Aegean Sea (Minoura et al., 2000; Wulf et al., 2002). One of the most conspicuous sediment types are sapropels. These layers formed during stagnation periods attributed to the impact of periodic climate changes of the borderlands (e.g., Rossignol-Strick, 1983; Rohling, 1994; Myers et al., 1998; Emeis et al., 2000; Stratford et al., 2000; Casford et al., 2003).

The warm and dry conditions in the Eastern Mediterranean Sea result in an intensive evaporation that exceeds precipitation and freshwater input from rivers. Thus, the salinity of the eastern Mediterranean Surface Water (MSW) rises to values >39‰, and the mean temperature is 16–25 °C (Wüst, 1961). Regional

hydrological contrasts and the prevailing wind system drive the general circulation pattern of the Aegean Sea that exhibits a counter-clockwise current of surface water (Fig. 1; Pickard and Emery, 1990). In more detail, this circulation is composed of several small-scaled eddies that change intensity and location with the seasonal wind field (Pinardi and Masetti, 2000; Lykousis et al., 2002). A total of 2–2.5 Sv of saline and warm surface and intermediate waters enter the Aegean Sea from the Levantine Sea through the Karpathos and Rhodes Straits and flow to the north along the western coast of Turkey (Balopoulos et al., 1999). South of the Dardanelles this water masses are diluted and diverted to the west by the inflow of low

saline (22–33‰) and cool (9–22 °C) Black Sea Water (BSW). This water moves west-northwest in the northern Aegean Sea and then towards the south and southwest along the coast of Greece (Pickard and Emery, 1990; Bayhan et al., 2001; Karageorgis et al., 2003).

3. Material, lithology and age model

Our investigations concentrate on two sediment cores that were recovered during cruise M51/3 of the German research vessel "Meteor" in the year 2001. Site GeoTü SL148 is situated in the northwestern Aegean Sea at 39° 45.23′N, 24° 05.78′E, in a water depth of 1094 m, whereas GeoTü SL123 has been taken in the southern Aegean Sea at 35° 45.33′N, 27° 33.34'E, in a water depth of 728 m (Fig. 1). We sampled the upper 332.5 cm of core SL148 with a spacing of 2.5 cm (140 samples) and the upper 473 cm of core SL123 with a spacing of 2 cm (235 samples).

The overwhelming part of the sediments recovered at the two sites consists of greyish brown muds. In general, they are moderately bioturbated, soft and water-rich. They contain minor nannofossils as well as traces of pteropods and foraminifers. Core tops at both sites contain basically undisturbed surface sediments as indicated by the presence of the oxidized layer. In both cores the sapropel S1 was recovered. The sapropel is an olive to olive grey organic-rich mud that contains minor nannofossils and traces of pteropods and foraminifers. In core SL148 the sapropel occurs at 136–109 cm, in core SL123 at 133–96 cm. A thin mud layer divides the sapropel in both cores into a lower layer S1a and an upper layer S1b. Both cores contain ash layers, which we identified based on their mineralogical

fingerprint (Druitt et al., 1999; Seymour et al., 2004) and on their position relative to ^{14}C datings (see below; Table 1). Core SL148 exhibits a greyish brown, moderately bioturbated ash layer at 355–340 cm. This ash is interpreted to represent the Y2-Tephra. Core SL123 shows two ash layers. The Y5-Tephra occurs at 410–378 cm, the Minoan Tephra at 55–52 cm.

We obtained age models for cores SL148 and SL123 by ^{14}C-accelerator mass spectrometry (AMS) dating (Table 1). The ^{14}C-dating was carried out on well-preserved shells of planktonic foraminifera (*G. ruber, G. bulloides, G. sacculifer, N. pachyderma dextral, T. quinqueloba*) that represent the age of the surface waters. Jorisson et al. (1993) justified this choice over monospecific dating. We applied an eastern Mediterranean reservoir age correction of 400 years (Siani et al., 2001) and converted the radiocarbon ages to calendar years using the publicly accessible version of the radiocarbon calibration software of Fairbanks et al. (2005). Additional age control points come from the S1-interruption that can be linked to the 8200 ka cold event (Sperling et al., 2003; Rohling and Pählike, 2005), from the Y2-Tephra in core SL148 (21.95 ka BP; Wulf et al., 2002), from the Minoan Tephra (3.65±0.20 ka BP; Hammer et al., 1987) and from the Y5-Tephra (37.100± 0.400 ka BP; Deino et al., 1994) in SL123.

According to the age model, the investigated interval of core SL148 has a basal age of 22 ka. The linear sedimentation rates are about 17 cm/ka in the late glacial and the sapropel intervals and about 14 cm/ka in the younger Holocene interval, providing a time resolution of 150 to 180 years with our samples. The basal age of core SL123 is approximately 42 ka. The sedimentation rates are approximately 11 cm/ka in the late glacial

Table 1
Data used for constructing the age model for the investigated cores GeoTü SL148 and GeoTü SL123

Core	Depth (cm)	Radiocarbon age (ka BP)	Calendar years (cal. ka BP)	Data	Reference
SL148	0.00		0.000	Sediment surface	
	71.25	4.750±0.040	4.899±0.057	^{14}C AMS dating	
	117.50		8.200	S1-interruption	a
	156.25	10.195±0.050	1.1217±0.027	^{14}C AMS dating	
	285.00	16.070±0.090	18.878±0.097	^{14}C AMS dating	
	348.00		21.950	Y2-tephra	b
SL123	0.00		0.000	Sediment surface	
	53.00		3.645±0.020	Minoan tephra	c
	96.00	6.655±0.035	7.191±0.050	^{14}C AMS dating	
	112.25		8.200	S1-interruption	a
	134.50	9.500±0.050	10.244±0.031	^{14}C AMS dating	
	221.00	17.180±0.090	19.948±0.162	^{14}C AMS dating	
	275.00	18.840+0.110/−0.100	22.419±0.083	^{14}C AMS dating	
	317.50	26.630+0.260/−0.250	31.306±0.212	^{14}C AMS dating	
	401.00		37.100±0.400	Y5-tephra	d

References: (a) Rohling and Pählike (2005), Sperling et al. (2003); (b) Wulf et al. (2002); (c) Hammer et al. (1987); (d) Deino et al. (1994).

interval, and approximately 13 cm/ka within the sapropel and the late Holocene interval, providing a time resolution of 160 to 190 years.

4. Methods

Bulk sediment samples of cores SL148 and SL123 were oxidized and disaggregated by means of a 5–10% H_2O_2 solution. Carbonate was removed by 10% acetic acid. Sieving the samples through a 63-µm mesh isolated the terrigenous sand fraction from the fine fraction. The clay fraction (<2 µm) was separated from the silt fraction by the Atterberg method. Clay/silt ratios were calculated.

The clay mineral composition was analysed by X-ray diffraction (XRD) of the clay fraction. The samples were mounted as texturally oriented aggregates and solvated with ethylene–glycol vapour at a temperature of 50°C. The analyses were conducted on a Rigaku MiniFlex system with CoKα radiation (30 kV, 15 mA). The

samples were X-rayed in the range 3–40° 2Θ with a step size of 0.02° 2Θ and a measuring time of 2 s/step. We additionally analysed the range 27.5–30.6° 2Θ with a step size of 0.01° 2Θ and a measuring time of 4 s/step in order to better resolve the (002) peak of kaolinite and the (004) peak of chlorite.

The individual clay minerals were identified by their basal reflections. For semiquantitative evaluations of the clay mineral assemblages, we used empirically estimated weighting factors on integrated peak areas of the individual clay mineral reflections (Biscaye, 1964, 1965; Brindley and Brown, 1980). The concentrations of smectite, illite, chlorite and kaolinite are given in percent of the total clay mineral assemblage.

The "crystallinity", a measure of the lattice ordering and crystallite size, is expressed as the integral breadth ($\Delta°2\Theta$) of the smectite 17 Å and illite 10 Å peaks. The integral breadth is the width of the rectangle, which has the same height and the same area as the measured peak. High values indicate poor crystallinities, whereas low
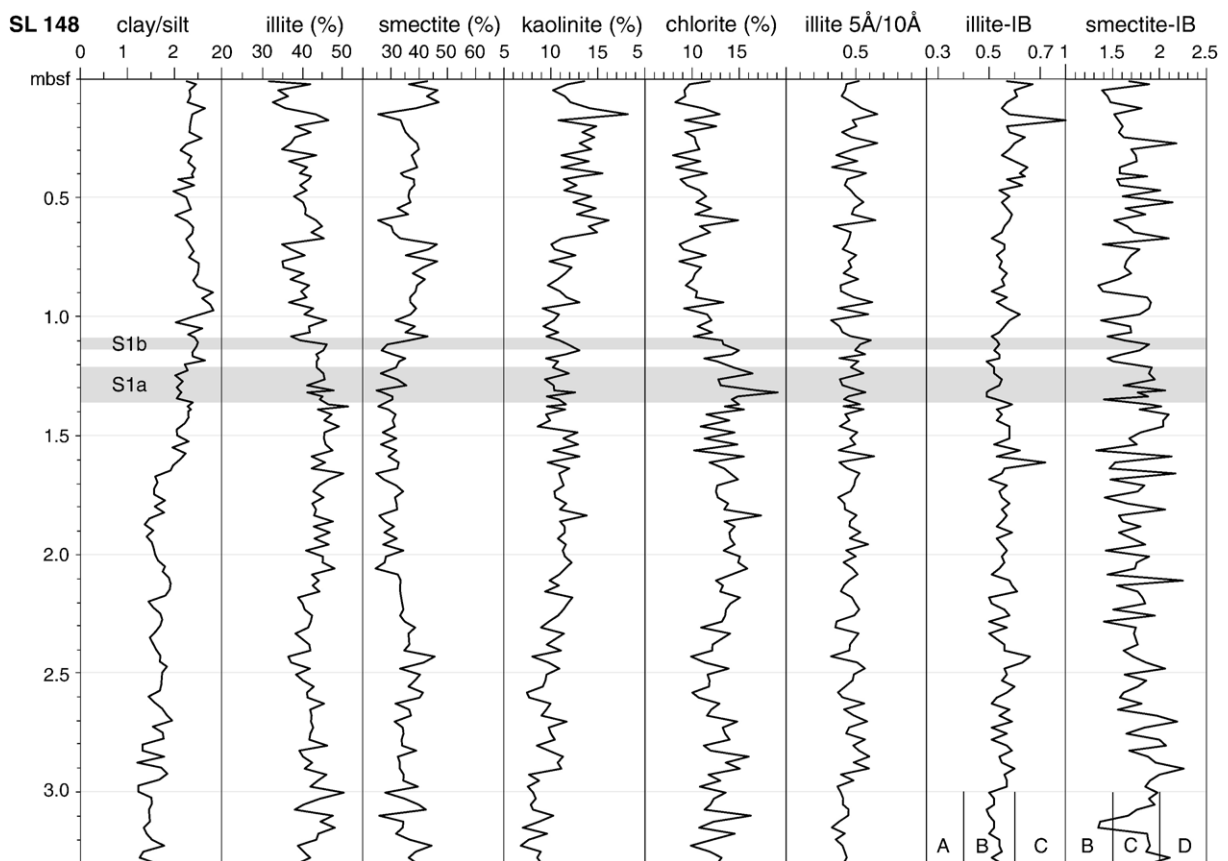

Fig. 2. Clay mineral data of core GeoTü SL148, northern Aegean Sea: clay/silt ratio, percentage distribution of the main clay mineral groups, illite 5 Å/10 Å peak areas and illite and smectite crystallinities (integral breadth, $\Delta°2\Theta$). Commonly used categories for very well crystalline (A), well crystalline (B), moderately crystalline (C) and poorly crystalline (D) are indicated.

values indicate good crystallinities. The illite chemistry was inferred from the 5 Å/10 Å peak area ratio. Al-rich illites (muscovite) have values >0.4, whereas Mg- and Fe-rich illites (biotite) have values <0.15 (Esquevin, 1969).

For Sr and Nd isotope analyses, 21 carbonate-free bulk sediment samples of core SL123 have been analysed following the procedures as described by Weldeab et al. (2002). The $^{87}Sr/^{86}Sr$ isotope ratios were normalised to $^{86}Sr/^{88}Sr = 0.1194$ and the $^{143}Nd/^{144}Nd$ isotope ratios to $^{146}Nd/^{144}Nd = 0.7219$. The La Jolla Nd-Standard yielded a mean value of 0.511814 ($n=4$, reference value 0.511850) and the NBS 987 Sr standard yielded $^{87}Sr/^{86}Sr$ ratios of 0.710250 and 0.71235 (reference value 0.710248). Total procedural blanks (chemistry and loading) were <200 pg for Nd and <200 pg for Sr. $^{143}Nd/^{144}Nd$ ratios are expressed as $\varepsilon_{Nd(0)}$, where $\varepsilon_{Nd(0)}$ are isotopic values normalized to the "chondritic uniform reservoir" value (0.512636) of Jacobson and Wasserburg (1980).

For evaluation of short-term fluctuations, the different time series have been detrended by subtraction of a 9-point least square smoothing. Blackman–Tukey spectral analysis was carried out on the detrended and normalized time series using the software AnalySeries 1.2 (version from 2/2000; Paillard et al., 1996). Prior to analysis, the records of SL148 and SL123 have been resampled with $\Delta t = 0.15$ ka and $\Delta t = 0.18$ ka, respectively.

All raw data presented in this study are available from the PANGAEA data bank of the Alfred Wegener Institute for Polar and Marine Research, Bremerhaven, Germany (http://doi.pangaea.de/10.1594/pangaea.586884).

5. Results

The results of the clay mineral analyses on sediments of cores SL148 and SL123 are shown in Figs. 2 and 3. The description given in this chapter therefore concentrates on the main features only.
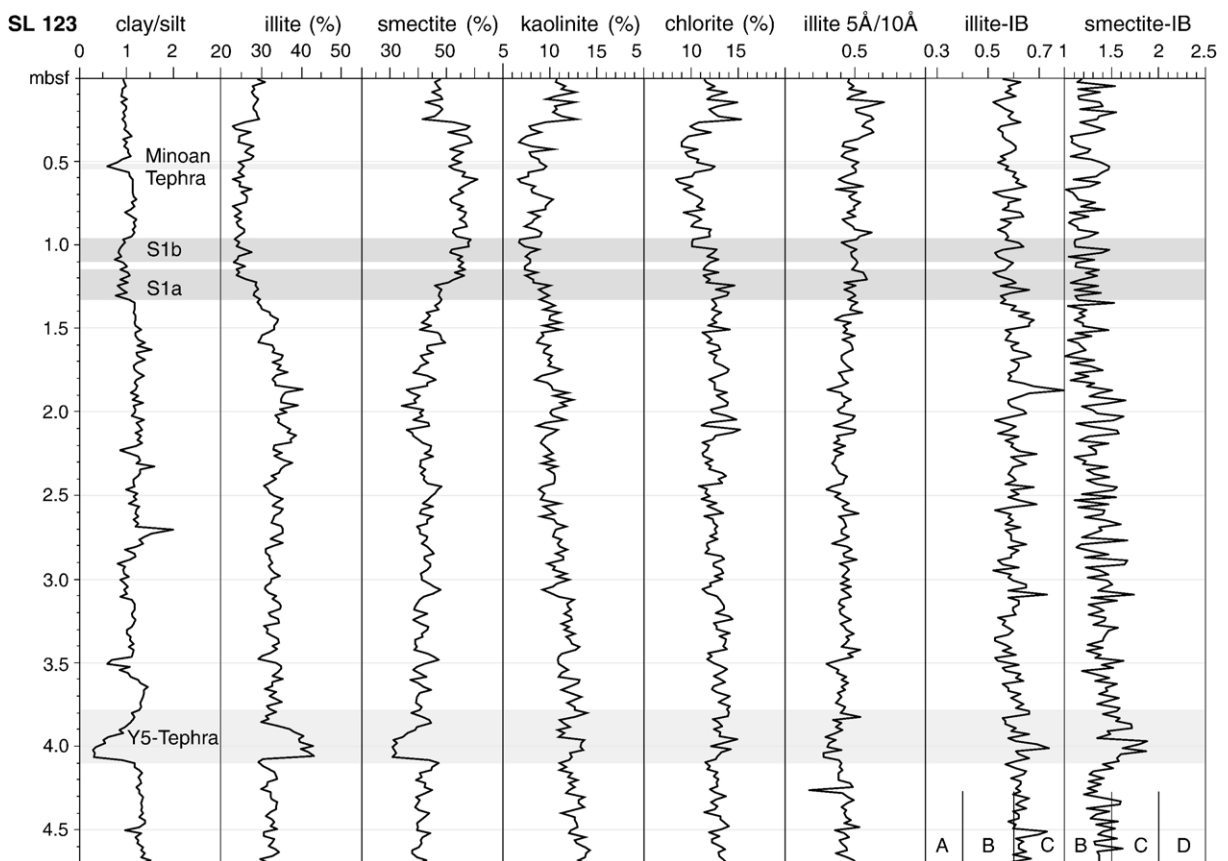

Fig. 3. Clay mineral data of core GeoTü SL123, southern Aegean Sea: clay/silt ratio, percentage distribution of the main clay mineral groups, illite 5 Å/10 Å peak areas and illite and smectite crystallinities (integral breadth, Δ°2Θ). Commonly used categories for very well crystalline (A), well crystalline (B), moderately crystalline (C) and poorly crystalline (D) are indicated.

The terrigenous clay/silt ratios in core SL148 range from 1.2 to 2.9. The values are relatively uniform at around 1.5 below 1.7 m below sea floor (mbsf). They increase between 1.7 mbsf and 1.2 mbsf to a level of about 2.3, which is maintained in the upper part of the core.

The illite concentrations fluctuate between 31% and 51% in core SL148. The distribution pattern is indistinct in the lower part of the core, with relatively high values around 3.0 mbsf and 2.0–1.5 mbsf. The concentrations generally decrease from ca. 45% to ca. 35% in the upper 1.5 m of the core. The smectite concentrations range from 25% to 47%. They show a slight decreasing trend from >40% to 30% between the bottom and 2.0 mbsf, relatively constant values of 30% at 2.0–1.3 mbsf, and generally somewhat higher but strongly fluctuating values of 30–45% in the upper part of the core. Kaolinite occurs in concentrations of 7–18%. The concentrations increase slightly from ca. 9% to ca. 12% between the bottom and 1.5 mbsf. They are relatively constant around 11% in the interval 1.5–0.7 mbsf. Above that level enhanced kaolinite contents can be observed. Chlorite occurs in similar concentrations as kaolinite, i.e. 8–19%. The distribution pattern seems somewhat diffuse but shows a trend of slightly increasing values from the bottom to ca. 1.2 mbsf and relatively low values of ca. 10% in the upper 1 m of the core.

The illite 5 Å/10 Å ratios vary between 0.32 and 0.65 without a systematic trend. They imply that the illites are relatively rich in Al and close to a muscovitic composition. Most illites in core SL148 have integral breadth values of 0.5–0.6 $\Delta°2\Theta$ and therewith are well crystalline. No trend is visible within the sequence. Although the integral breadth values of smectite are strongly fluctuating, most of the smectites are moderately crystalline (1.5–2.0 $\Delta°2\Theta$). A weak trend to slightly better crystallinities towards the top of the core can be observed.

The terrigenous clay/silt ratios in core SL123 are distinctly lower and more constant than in core SL148. They generally range between 0.9 and 1.2. A weak trend to lower values develops within the core. Several excursions from this trend can be observed. The Y5-Tephra and the Minoan Tephra show distinctly lower values, and sapropel S1 shows slightly lower values.

The illite concentrations in core SL123 are lower than in core SL148 and fluctuate between 23% and 43%. From the bottom to 1.8 mbsf the concentrations increase slightly from 30% to 35%. The Y5-Tephra within this interval shows enhanced illite concentrations of up to 42%. Within the interval 1.8–1.3 mbsf the concentrations decrease to a level of 25%, which is maintained up to 0.2 mbsf. The uppermost few samples have ca. 30% illite.

The smectite concentrations of 31–61% are higher than in core SL148. Relatively homogenous concentrations of around 40% are found in the lower part of the core. From 1.8 mbsf to the top of the core, the concentration pattern is opposite to that of illite. Kaolinite and chlorite occur in similar concentrations as in core SL148. The kaolinite content is 7–14%. The lower part of the core, up to ca. 1.3 mbsf, shows a general decrease in kaolinite concentrations from ca. 14% to ca. 9%. The interval 1.3–0.2 mbsf has generally lower but strongly fluctuating concentrations. High concentrations of 10–13% occur in the uppermost 20 cm of the core. Chlorite shows similar amounts as kaolinite, but instead of a decreasing trend in the lower part of the core, it there exhibits relatively constant concentrations of ca. 12%.

Similar as in core SL148, the 5 Å/10 Å ratios in core SL123 vary between 0.3 and 0.6, with a trend to slightly higher values in the upper part of the core. The illites are relatively rich in Al and close to a muscovitic composition. The illites have integral breadth values that are only slightly higher than in core SL148. Most values are between 0.5 $\Delta°2\Theta$ and 0.65 $\Delta°2\Theta$. Thus, most illites are well crystalline. The crystallinity improves slightly upcore. The integral breadth values of smectite fluctuate between 1.0 $\Delta°2\Theta$ and 1.9 $\Delta°2\Theta$. The data show a transition from well to moderately crystalline smectites in the lower part to well crystalline smectites in the upper part of the core. Thus, the

Table 2
Sr- and Nd-isotopic composition of carbonate-free bulk sediment samples from core GeoTü SL123

Depth (cm)	$^{87}Sr/^{86}Sr$ ($\pm2\sigma \times 10^{-6}$)	$^{143}Nd/^{144}Nd$ ($\pm2\sigma \times 10^{-6}$)	$\varepsilon_{Nd(0)}$
1	0.714882 (10)	0.512186 (09)	−8.8
5	0.713962 (08)	0.512197 (07)	−8.6
9	0.712630 (08)	0.512193 (10)	−8.7
13	0.712899 (10)	0.512210 (07)	−8.3
17	0.714222 (08)	0.512212 (09)	−8.3
21	0.713826 (07)	0.512206 (08)	−8.4
25	0.713406 (09)	0.512204 (08)	−8.5
29	0.714066 (10)	0.512233 (08)	−7.9
33	0.713448 (10)	0.512207 (10)	−8.4
37	0.713539 (08)	0.512177 (08)	−9.0
41	0.714896 (07)	0.512205 (09)	−8.4
45	0.712276 (10)	0.512213 (07)	−8.3
49	0.712441 (09)	0.512283 (06)	−6.9
53	0.711772 (10)	0.512289 (07)	−6.8
57	0.712997 (10)	0.512238 (08)	−7.8
61	0.714271 (09)	0.512236 (09)	−7.8
65	0.711602 (10)	0.512233 (07)	−7.9
69	0.711491 (07)	0.512227 (08)	−8.0
73	0.712287 (09)	0.512214 (07)	−8.3
77	0.712123 (10)	0.512225 (08)	−8.1
81	0.712490 (08)	0.512248 (10)	−7.6

smectites are generally better crystalline than that of core SL148.

Also the kaolinite shows a distinctly different XRD pattern. In the northern core, the kaolinite and chlorite reflection at ca. 7.14 Å overlap to a single and sharp peak. In contrast, the reflections in the southern core show two separate peaks at 7.27 Å (001 kaolinite) and at 7.13 Å (002 chlorite), or a peak at 7.13 Å with a shoulder at 7.27 Å. This pattern is visible in both the air-dried and the glycolated samples, which implies that it is not caused by the presence of mixed-layered clay minerals with smectite as one component. We assume that this XRD pattern is caused by a very good crystallinity of the kaolinite or by a different chemical composition.

Palygorskite was identified in samples of core SL123. Because of its low concentration, however, the diffractograms show no distinct peak but only a slight shoulder at 10.4 to 10.5 Å accompanying the 10 Å illite peak. Therefore, quantification was not possible.

The $^{87}Sr/^{86}Sr$ values in core SL123 range between 0.711491 and 0.714896 and show a slight increasing trend towards the top of the core; the $^{143}Nd/^{144}Nd$ values range between 0.512177 and 0.512289 and show a slight decreasing trend (Table 2).

6. Discussion

The distribution of individual clay minerals in the surface sediments of the Aegean Sea allows the discrimination of six provinces (Ehrmann et al., in press). They reflect different source areas and the distribution of suspended matter by ocean currents (Fig. 4). The provinces mainly differ in respect to their smectite versus illite contents. Illite is for the most part
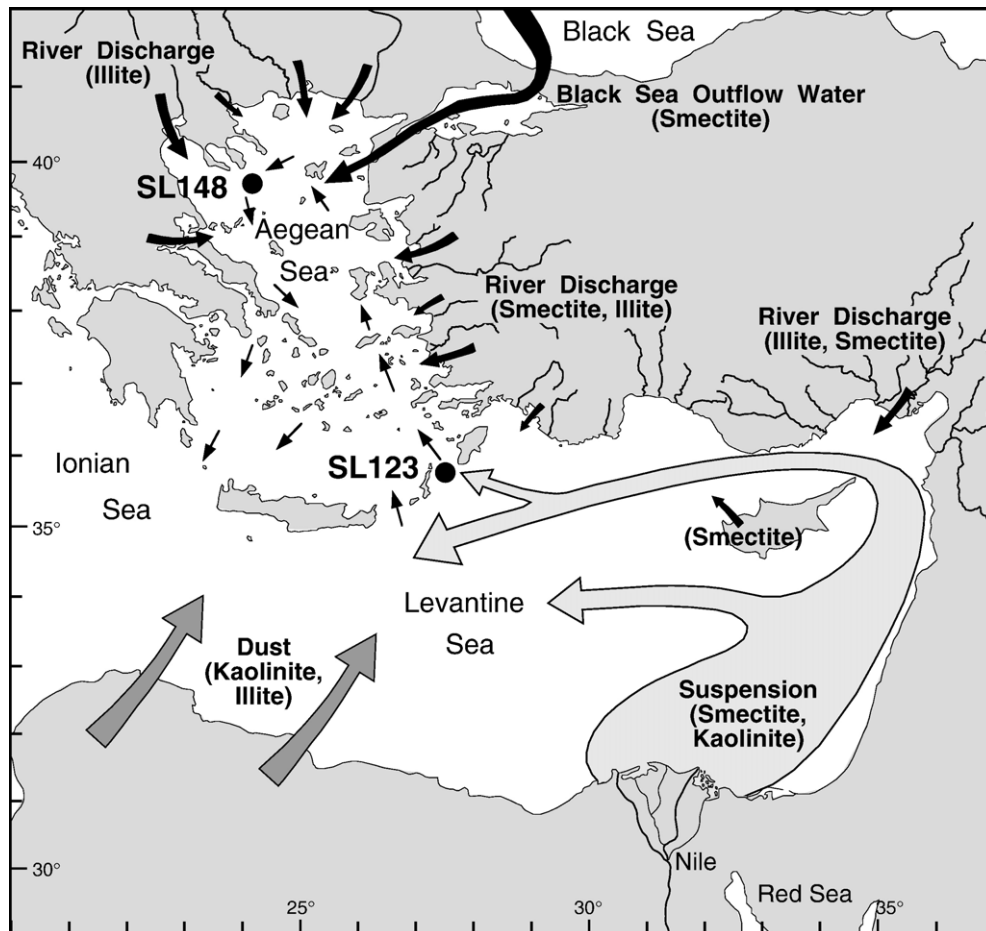

Fig. 4. Compilation of present-day source areas, transport processes and transport paths for the major clay mineral groups in the Eastern Mediterranean Sea (after Ehrmann et al., in press). The clay minerals of the northern Aegean Sea are mainly derived by river discharge. In contrast, the clay mineral assemblages in the southernmost Aegean Sea and Levantine Sea are mainly controlled by the suspension load of the Nile and by aeolian influx. The positions of the investigated cores GeoTü SL148 and GeoTü SL123 are indicated.

derived from the rivers discharging into the northwestern and northern Aegean Sea. Smectite is mostly derived from sources in the Dardanelles–Marmara Sea region, West Turkey and possibly also from surface currents transporting suspensions from the Nile River towards the southern Aegean Sea. Therefore, the smectite/illite ratio is regarded as a suitable proxy for reconstructing the influence of the different source areas through time. Furthermore, the smectite/illite ratio is promising for reconstructing palaeoclimate, because smectite normally forms by chemical weathering under a warm and humid climate, whereas illite normally forms by physical weathering under a cool and dry climate.

The kaolinite/chlorite ratio is another important parameter for reconstructing palaeoenvironment although both minerals occur only in minor concentrations in surface sediments of the Aegean Sea (Ehrmann et al., in press). The ratio is controlled by climate and source area. Chlorite normally results from physical weathering, but is not resistant against chemical weathering and transport. Chlorite occurs in minor concentrations throughout the Aegean Sea without showing a dominant source. Kaolinite is normally derived from chemical weathering and requires humid and warm conditions for its formation. High concentrations are mainly restricted to regions, where long-lasting and intense hydrolysis and lateritic soil formation occurs. Because kaolinite is very resistant, it may be reworked from older sedimentary rocks or soils. The North African continent is an important source for kaolinite, which is transported by wind and/or by the river Nile towards the Eastern Mediterranean and then is distributed by ocean currents (Venkatarathnam and Ryan, 1971; Chester et al. 1977; Foucault and Mélières, 2000).

At present, the two sites in the northernmost and southern Aegean Sea belong to different clay mineral
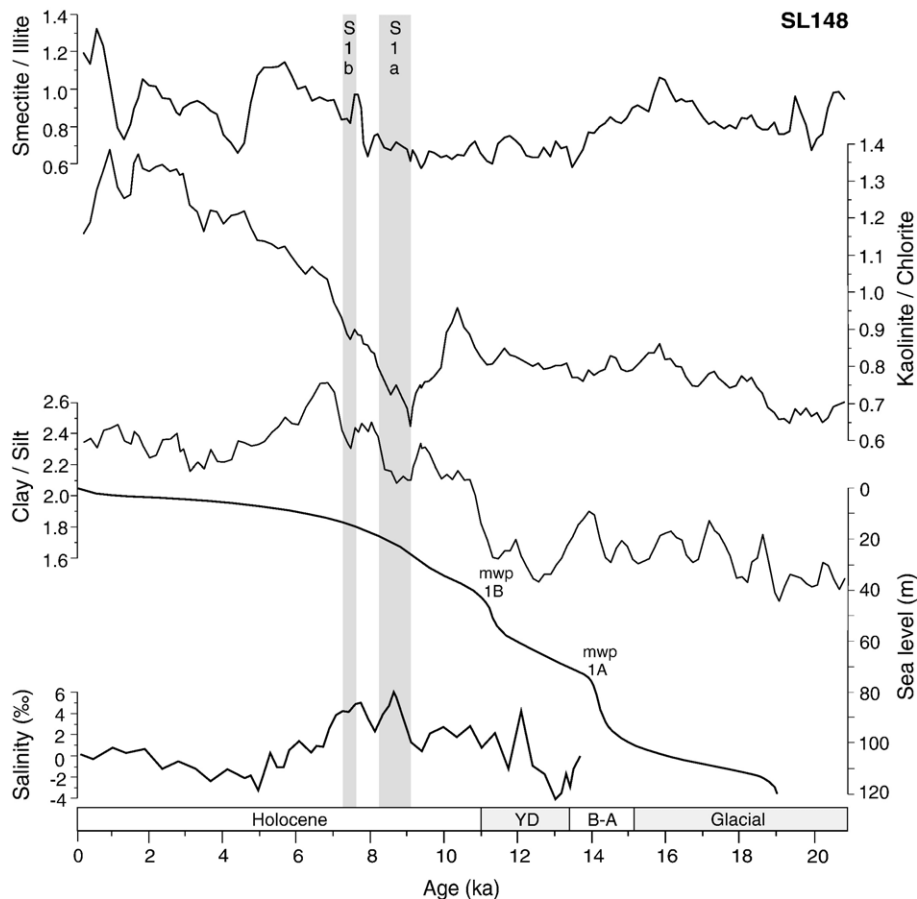

Fig. 5. Late glacial to present variations in the ratios smectite/illite, kaolinite/chlorite and clay/silt in core GeoTü SL148, northern Aegean Sea (3-point-running means). Grey bars indicate the sapropel layers S1a and S1b. The sea level curve (m below present level; Bard et al., 1990) and the salinity curve of the Marmara Sea (compared to modern; Sperling et al., 2003) are shown for comparison. Mwp = meltwater pulse, YD = Younger Dryas, B–A = Bølling–Allerød.

provinces (Ehrmann et al., in press). Site SL148 belongs to the Central Aegean Province. This province is characterised by 30–35% illite, 40–45% moderately crystalline smectite, 15% kaolinite and 10% chlorite providing a mixed provenance and dispersal signal. Smectite-rich assemblages are delivered from the Marmara–Dardanelles and the West Turkey provinces by the counter-clockwise surface currents. Illite-rich assemblages are derived from the Northwest Aegean Province, which is characterised by an illite-rich river runoff from southern Europe. In contrast, the southern site SL123 belongs to the Southeast Aegean Province. This province is characterized by 25–35% illite, 35–50% well crystalline smectite, ca. 15% kaolinite and ca. 12% chlorite, and reflects a combination of transport by ocean currents and aeolian input (Venkatarathnam and Ryan, 1971; Ehrmann et al., in press). The temporal variability in grain size distribution and clay mineral assemblages of the Aegean Sea (Figs. 5 and 6) suggests that a series of palaeoclimatic and

palaeoceanographic changes have taken place during the last 42 ka. In addition, substantial differences in sediment grain size between the northern and southern Aegean Sea implies that different processes controlled the sedimentation in the two regions.

6.1. Processes controlling input and dispersal of terrigenous sediments

6.1.1. Deglaciation, sea level and ocean circulation

The clay mineral assemblages and the grain size distribution of the northern Aegean Sea were controlled by the late Quaternary deglaciation, the sea level rise and the associated oceanic circulation changes.

The low clay/silt ratios of ca. 1.5 in the glacial part of core SL148 (Fig. 5) are much lower than at present time and result from a transport of coarse sediment particles to the sampling site. In the same interval the smectite/illite ratios fluctuate around a mean of ca. 0.8, compared
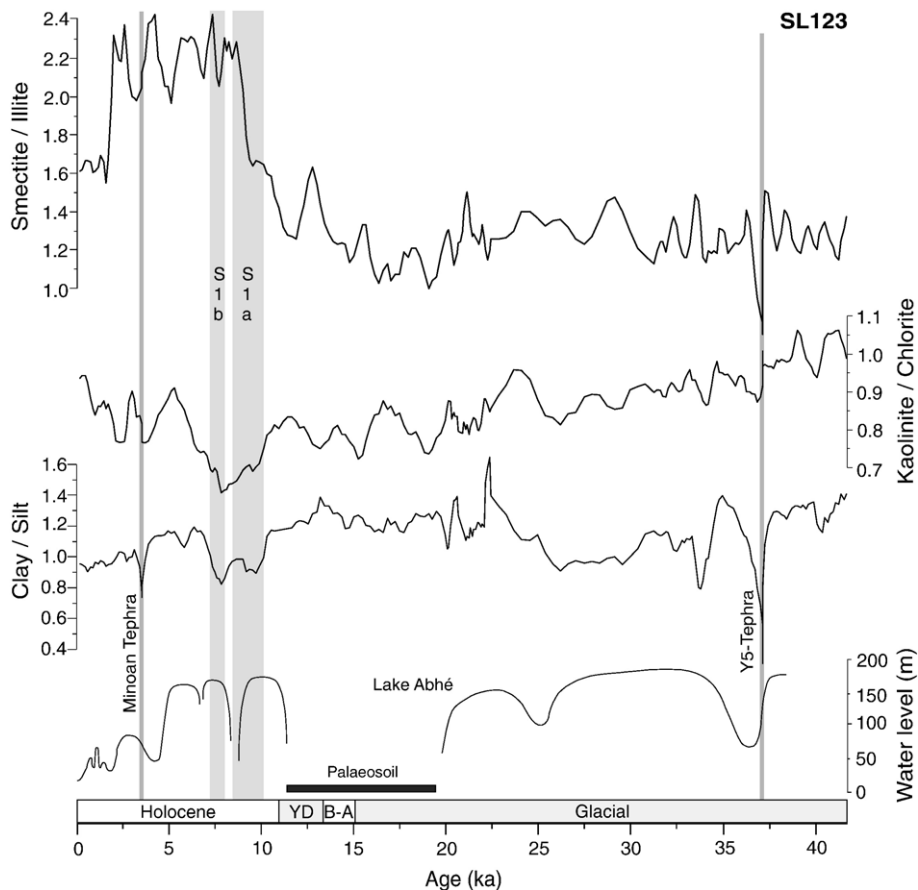

Fig. 6. Glacial to present variations in the ratios smectite/illite, kaolinite/chlorite and clay/silt in core GeoTü SL123, southern Aegean Sea (3-point-running means). Grey bars indicate the sapropel layers S1a and S1b. The lake-level curve of Lake Abhé in Ethiopia (m above present level; Gasse, 2000) is shown for comparison. YD=Younger Dryas, B–A=Bølling–Allerød.

to ca. 1.2 at present-day. During the LGM, sea level was ca. 120 m lower than today (e.g., Bard et al., 1990). The topography of the northern Aegean Sea suggests that large shelf areas were exposed and that several rivers discharged directly to the deeper basins during periods of high precipitation (Cramp et al., 1988; Perissoratis and Conispoliatis, 2003). Coarse particles were possibly also transported by wind. In addition, the exchange of surface water masses with the Levantine Sea was likely restricted and the Black Sea was totally isolated from the Aegean Sea (Sperling et al., 2003). Thus, the delivery of smectites was restricted. The climatic conditions were generally drier and colder than today (e.g., Mommer-steeg et al., 1995) and thus hampered smectite formation by chemical weathering, but favoured illite and chlorite formation by physical weathering. Episodic or periodic rivers obviously discharged into the sea and delivered high concentrations of illite. Because of the low sea level, the rivers brought the clay minerals close to the site. In contrast, at present-day a large proportion of the river-transported illite is trapped on the shelf areas (Poulos et al., 1996; Karageorgis et al., 2005) and characterizes the Northwest Aegean Province (Ehrmann et al., in press). The glacial interval of core SL148 exhibits also very low kaolinite/chlorite ratios (Fig. 5). The dry conditions may have allowed a transport of kaolinite by wind to the Eastern Mediterranean Sea (see Section 6.1.3). From there, however, kaolinite was not transferred to the northern Aegean Sea, because the low sea level hampered the oceanic transport.

The increase in the clay/silt ratios after the LGM (Fig. 5) documents the sea level rise caused by the melting of continental ice masses. Towards the end of the glacial period, the sediment grain size decreased slightly. The slowly submerging shelf areas started to trap the coarser sediment particles (Perissoratis and Conispoliatis, 2003) and only the smaller particles reached the sampling site. The following stepwise decreases in grain size document meltwater pulse 1A, which is centred at 14.0 ka and caused a sea level rise to − 70 m, and meltwater pulse 1B, which is centred at 11.3 ka and caused a sea level rise to − 40 m (Bard et al., 1990). The fining trend was interrupted during the Younger Dryas, when sediments in the northern Aegean Sea coarsened again. This may be due to a temporary return to cold, near-glacial conditions. The Younger Dryas was generally an arid period in the Mediterranean area (e.g., Bottema, 1995; Gasse, 2000). The change in the vegetation cover may have been responsible for enhanced erosion and transport of coarser sediments. Additionally, aeolian transport may have been responsible for the coarser grain sizes.

The increasing kaolinite/chlorite ratios also record the post-glacial sea level rise by implying an oceanic transport of kaolinite from the Levantine Sea and the southern Aegean Sea to the sampling site. This seems more likely than a local kaolinite source, because the kaolinite distribution in the surface sediments does not display a distinct kaolinite source on the surrounding land masses and because the kaolinite/chlorite ratio of near-shore sites is not distinctly higher than that at site SL148 (Ehrmann et al., in press). Also increased amounts of smectite should have been transported northward with the establishment of the modern Aegean surface currents, but the smectite/illite ratio of core SL148 reveals a more complicated pattern. Meltwater pulse 1A is likely responsible for a decrease in smectite/illite ratios between 16 ka and 13.5 ka. Most of the meltwater entering the Aegean Sea came from the north and resulted from melting of ice masses of the Rhodope mountains (Fig. 1). Thus, the rivers of the Northwest Aegean Province provided high amounts of illite-dominated clay during this period. Smectite/illite ratios remained almost constant at ca. 0.6 to 0.8 until ca. 8 ka. This implies that river discharge was high throughout this interval as a result of continued deglaciation in Europe and that this was a major source for clay minerals in the northern Aegean Sea.

During the early Holocene, sedimentation in the northern Aegean Sea was influenced by the stagnation period of sapropel S1 between approximately 10 and 7 ka and by the establishment of the connection between Aegean Sea and Black Sea. Core SL148 documents two coarsening episodes, during the sedimentation of sapropel layers S1a and S1b (Fig. 5). They may be due to more humid conditions with enhanced rainfall and river runoff in the northern Aegean Sea region and therefore influx of coarser material (Rossignol-Strick et al., 1982; Cramp et al., 1988; Rohling and Hilgen, 1991; Aksu et al., 1999). During S1 deposition less kaolinite was provided by erosion because of denser vegetation cover as a result of more humid conditions. Furthermore, ocean circulation was sluggish (Cramp et al., 1988; Myers et al., 1998; Stratford et al., 2000; Casford et al., 2003) and less suspension could therefore be transported to the northern Aegean Sea.

The smectite/illite ratios increased between 8 ka and 6 ka (Fig. 5). This increase can be attributed to a combination of two different processes. The first process links the Holocene increase in smectite concentrations to the opening of the oceanic gateway between the Marmara Sea and the Black Sea at ca. 8 ka (Ryan et al., 1997; Ballard et al., 2001; Sperling et al., 2003). Although the gateway between the Aegean Sea

and the Marmara Sea had opened at ca. 13.5 ka (Sperling et al., 2003), we assume that a notable inflow of water from the Marmara Sea into the northern Aegean Sea was not possible until the connection to the Black Sea had established. Because the surface sediments in the Marmara–Dardanelles Province are rich in smectite (Ehrmann et al., in press), the inflow water should carry high concentrations of smectite. The inflow water is diverted towards the northern Aegean Sea (Fig. 1) and thus may transport smectite to the sampling site, although its total suspension load is low at present-day. Theoretically, smectite could also be derived from surface currents flowing from the West Turkey Province to the north (Ehrmann et al., in press).

The second process links the generally higher Holocene smectite concentrations to the climatic evolution. The Holocene climatic trend resulted in warmer and more humid conditions. This trend was followed by a change in the weathering regime and the establishment of chemical weathering conditions that allowed the formation of smectite. Rivers transported the smectites into the Aegean Sea. Although highest humidity and river runoff occurred during the formation of the sapropel layer (e.g., Rohling and Hilgen, 1991; Aksu et al., 1999), the sapropel at SL148 does not show enhanced smectite concentrations, because the connection to the Black Sea was not yet established at that time. This is a further indication for a significant Black Sea influence on the middle to late Holocene smectite/illite ratios in the northern Aegean Sea.

Since about 7 ka the late Holocene proxy records clearly differ from the record of the sea level (Fig. 5), which had reached almost its present position at 7 ka (−12 m; Bard et al., 1990). This indicates that other processes controlled sedimentation in the northern Aegean Sea. It is striking that the clay/silt ratio in this time interval correlates well with the salinity record of the Marmara Sea (Sperling et al., 2003). The salinity in the Marmara Sea is controlled by the outflow of Black Sea Water. After the filling of the Black Sea had been completed some 8–7 ka ago, surface water intruded from the Black Sea into Marmara and Aegean seas leading to a decrease in surface water salinity. The outflow reached a maximum at around 5–4 ka and afterwards decreased slightly to present-day values (Sperling et al., 2003). This trend is also visible in the clay/silt ratios and in maximum smectite/illite ratios (Fig. 5). Minor discrepancies between the different curves may be due to different age models. Today, the low salinity tongue originating from the outflow of the Black Sea can be traced throughout the northern Aegean Sea (Fig. 1; Aksu et al., 1995). The Black Sea Water

does not bring much suspension. Thus, the sediment influx through the Dardanelles Strait is negligible, if compared with the river discharge into the northern Aegean Sea (compilation in Ehrmann et al., in press). However, the outflow of Black Sea Water into the Aegean Sea may have changed the oceanographic regime, and, therefore, the grain size and smectite/illite curves from core SL148 may document the establishment of the modern circulation in the northern Aegean Sea. In the late Holocene clay mineral record of this core two very prominent incursions with strongly reduced smectite/illite ratios are attributed to abrupt climate change of the northern borderlands (see Section 6.2).

In the southern Aegean Sea core SL123 terrigenous sedimentation patterns (Fig. 6) cannot be related to the sea level curve. The sediments are generally coarser than at the northern site SL148. The core site is far off the continent, close to the islands of Rhodes and Karpathos. The shelves of the islands are very narrow (Perissoratis and Conispoliatis, 2003). Therefore the exposure and flooding of the continental or island shelves with changing sea level did not influence the sediment supply to the site. Sediment supply by rivers was less important in this region, because no major rivers are present in the vicinity of the site (Fig. 1). The coarser size of the terrigenous sediment particles may be explained by deposition in a shallower water depth of 728 m, compared to 1094 m at the northern site. The islands of Rhodes and Karpathos may serve as proximal sediment sources. Furthermore, aeolian dust from the North African desert is a significant constituent of the marine sediments in the Eastern Mediterranean Sea (Venkatarathnam and Ryan, 1971; Pye, 1992) and may also be responsible for the coarser grain size at the sampling site (see Section 6.1.3). Finally, redistribution and sorting of the sediments by bottom currents may have influenced the grain size. Because so many different processes may have been active, the observed pattern in the clay/silt ratio cannot be interpreted unequivocally. However, it is obvious that large fluctuations occurred during the glacial phase and indicate quite unstable sedimentary conditions. In contrast, only small fluctuations occurred between some 20 and 10 ka and after 7 ka (Fig. 6). Similar as in the northern Aegean Sea, the sapropel layers S1a and S1b are distinctly coarser than the surrounding sediments reflecting enhanced river runoff during a humid climate.

Based on their modern distribution patterns (Venkatarathnam and Ryan, 1971; Bayhan et al., 2001; Ehrmann et al., in press) the clay minerals of core SL123 reflect a combination of transport by ocean

currents and aeolian input from the Sahara (Fig. 4). Surface and intermediate water masses enter the Aegean Sea through the Rhodes and Karpathos straits, as part of the large-scale oceanic circulation pattern of the Eastern Mediterranean Sea (Balopoulos et al., 1999). Consequently, the smectite/illite ratio likely represent a distal signal of Nile suspended material (see Section 6.1.2). In contrast, the kaolinite/chlorite ratio, which shows a distribution pattern independent from the smectite/illite ratio, primarily reflects changes in North African aridity and southern Mediterranean wind speed (see Section 6.1.3; Venkatarathnam and Ryan, 1971; Foucault and Mélières, 2000).

6.1.2. Nile discharge and suspension load

The southern core SL123 shows smectite/illite and kaolinite/chlorite patterns that are distinctly different from that in the northern Aegean Sea (Fig. 6). The smectites are better crystalline at site SL123 than at the northern site SL148 (Figs. 2 and 3). This implies a

different source. A northern source is not very likely, because at the site surface currents flow northward into the Aegean Sea and the outflow of water and dispersion of lithogenic components from the Aegean Sea is mainly through the Strait of Casos between Crete and Karpathos, and through the Kithira Strait (Fig. 1; Balopoulos et al., 1999; Weldeab et al., 2002). Therefore, a large proportion of the smectite probably is derived from the south or southeast by surface currents and ultimately originates from the River Nile (Fig. 4). The Nile discharges ca. 160×10^6 t/yr suspension load with a clay mineral composition of some 60% well crystalline smectite, 30% kaolinite and 10% illite (Venkatarathnam and Ryan, 1971; Stanley and Wingerath, 1996). The smectite is derived from the Blue Nile and Atbara River and has its source in the Cenozoic volcanic terrains of the Ethiopian Plateau, where the humid climate favours its formation. From the river mouth, the smectite is transported with the counterclockwise surface currents along the coasts of Israel,
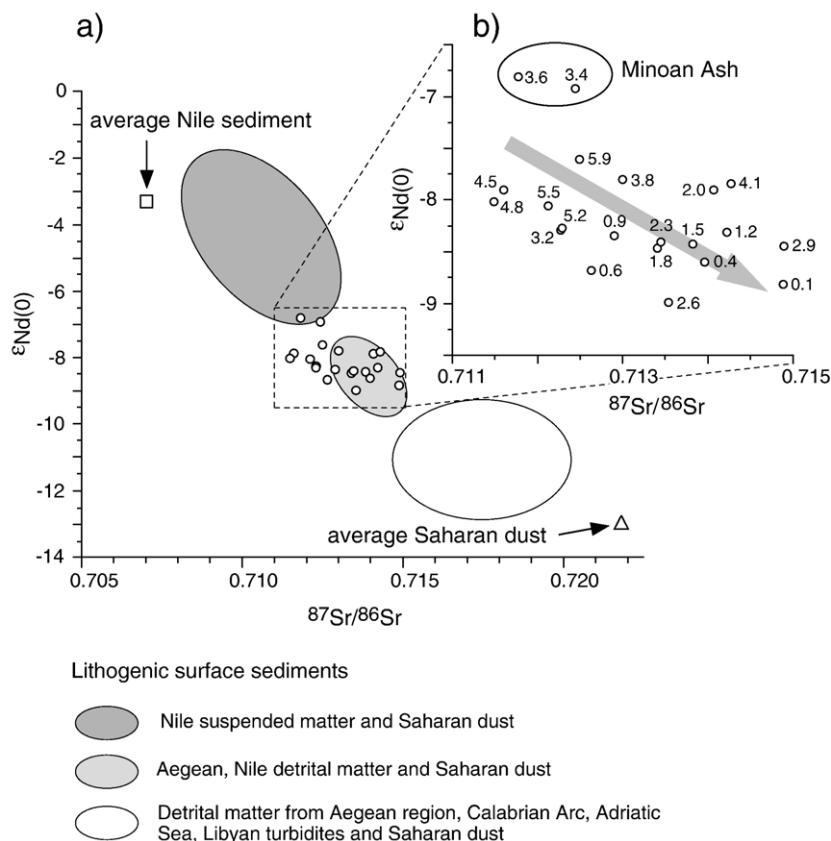

Fig. 7. $^{87}Sr/^{86}Sr$ ratios versus $^{143}Nd/^{144}Nd$ ratios, expressed as $\varepsilon_{Nd(0)}$ values, of a) lithogenic surface sediments from the Eastern Mediterranean Sea, as well as of genuine Saharan dust and Nile sediments (as compiled by Weldeab et al., 2002) and b) late Holocene sediments of core GeoTü SL123 from the southern Aegean Sea. Shaded areas and accompanying text indicate provenance and main sources of terrigenous components. Numbers in b) denote interpolated ages in ka, reflecting an overall decrease of $\varepsilon_{Nd(0)}$ values and increase of $^{87}Sr/^{86}Sr$ ratios during the past 6 ka.

Lebanon, Syria and Turkey towards the South Aegean Sea (Venkatarathnam and Ryan, 1971; Foucault and Mélières, 2000). According to Krom et al. (1999), 10–15% of the carbonate-free suspension load of the Nile reaches the northwestern Levantine Sea close to our sampling site. The distribution patterns of $^{87}Sr/^{86}Sr$ and $^{143}Nd/^{144}Nd$ in surface sediments further supports the idea of a long-distance transport of suspension from the Nile at least to the northern Levantine Sea (Krom et al., 1999; Weldeab et al., 2002). Our own $^{87}Sr/^{86}Sr$ and $^{143}Nd/^{144}Nd$ data indicate that the Holocene sediments at site SL123 are a mixture of Aegean components, Nile detrital matter and Saharan dust (Fig. 7).

The smectite/illite ratios in core SL123 were relatively low between 42 ka and 15 ka (Fig. 6). They indicate that smectite formation on land was not effective and/or that the influx of smectite into the Mediterranean Sea was reduced. This finding is consistent with the cold and dry climate during the

late Pleistocene period. The hyper arid interval of the LGM shows the lowest smectite/illite ratios (Fig. 6). The sediment discharge of the Nile was distinctly reduced during the time interval 25–12.5 ^{14}C ka and the Nile was probably a highly seasonal braided river. Although flood peaks were high, the annual discharge was low (Adamson et al., 1980).

The smectite/illite ratios of core SL123 started to increase at ca. 14.5 ka indicating higher smectite formation and/or influx, probably through the Nile. The increase occurred at the time, when humid conditions commenced after the full glacial hyper arid conditions during the latest Pleistocene (COHMAP Members 1988; deMenocal et al., 2000) and when also lake basins began to fill and expand in the formerly arid regions (e.g., Gasse, 2000). This major climatic change was synchronous with the end of cold, glacial conditions in Europe. However, the smectite/illite ratios decreased temporarily at the time of the Younger Dryas, between
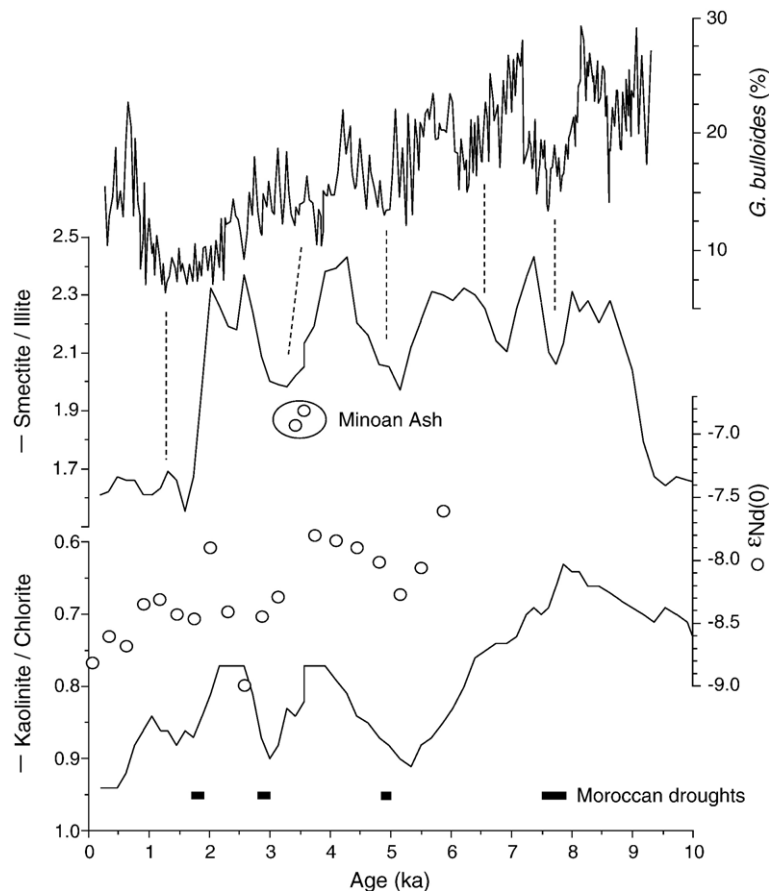

Fig. 8. Smectite/illite and kaolinite/chlorite ratios (3-point-running means) versus $^{143}Nd/^{144}Nd$ ratios, expressed as $\varepsilon_{Nd(0)}$ values (circles) of Holocene lithogenic sediments of core GeoTü SL123 from the southern Aegean Sea. Indian monsoon intensity as indicated by the relative abundance of the upwelling indicator *Globigerina bulloides* (Gupta et al., 2005) is shown for comparison. Intervals of decreased monsoon intensity correspond to dry phases in East and North Africa. Black bars indicate arid intervals in the Middle Atlas of Morocco (Lamb et al., 1995).

ca. 12.5 ka and 10.5 ka (Fig. 6). The Younger Dryas interrupted the establishment of humid conditions and was associated with a sharp increase in regional aridity (e.g., Lamb et al., 1995; Gasse, 2000), which resulted in less smectite formation and transport.

The most dramatic increase in smectite/illite ratios occurred at ca. 9 ka and documents a major change in climate and in sediment input by the Nile. It happened shortly after the onset of the so-called African Humid Period, which lasted until 6 ka. The Sahara was nearly completely vegetated during the African Humid Period and numerous lakes existed in subtropical North Africa (Fig. 6; Street and Grove, 1976; COHMAP Members, 1988; Kutzbach et al., 1996; Gasse, 2000). The present-day flow regime of the Nile established with the onset of humid conditions at the beginning of the Holocene (Talbot et al., 2000; Krom et al., 2002). This resulted in a permanent and more regular flow of the river (Adamson et al., 1980). Furthermore we assume that more smectite could be formed in the Ethiopian source area because the climate favoured chemical weathering. Thus, more smectite was transported by the Nile to the Eastern Mediterranean Sea, where it was distributed by surface currents.

The late Pleistocene to Holocene humid phase was linked to an intensification of the African monsoon due to earth orbital changes, which increased summer season insolation. More humid conditions established at 14.5 ka, when boreal summer insolation (calculated for 20°N) crossed a threshold value, which was 4.2% greater than present (deMenocal et al., 2000). Insolation reached a maximum at 11–10 ka. The previous insolation maximum, however, does not find expression in the clay mineral data, probably because it was less pronounced and because it occurred under glacial boundary conditions. Thus, because of the weaker monsoon, Nile discharge was much less and, therefore, also sapropel S2 is only poorly developed in the Eastern Mediterranean Sea (Cramp and O'Sullivan, 1999).

It is not yet understood, why the smectite/illite ratios do not mirror the end of the African Humid Period some 5 ka ago. One could speculate that the climate in the source area of the smectite, in the Ethiopian Highland, was decoupled from the North African climate and instead was influenced by the Indian monsoon (Fig. 8). The drastic decrease in the smectite/illite ratio at ca. 2 ka may be due to a fall of the humidity below a certain threshold or to anthropogenic influences.

6.1.3. Aeolian sediment input from North Africa

Satellite images and sedimentological observations show that large amounts of dust are presently trans-ported with southwesterly Scirocco winds from the Sahara into the eastern Mediterranean area including the southern Aegean Sea (Tomadin et al., 1984; Bolle, 2003). In contrast, direct input of aeolian particles to the northern Aegean Sea is quantitatively negligible if compared with the sediment input by rivers (Chester et al., 1977; Kubilay et al., 1997). The aeolian sediment material contains up to 50% kaolinite (Chester et al., 1977; Stanley and Wingerath, 1996) and bears a distinctive geochemical signature, i.e. high $^{87}Sr/^{86}Sr$ and low $^{143}Nd/^{144}Nd$ ratios (Fig. 7; Weldeab et al., 2002; Frumkin and Stein, 2004).

In the surface sediments of the Aegean Sea, no distinct source area for kaolinite is obvious. However, kaolinite concentrations seem especially low in the Northwest Aegean Province, but slightly enhanced in the West Turkey Province and the Central Aegean Province (Ehrmann et al., in press). This indicates transport of kaolinite with ocean currents to site SL148. Kaolinite can be fed into the oceanic system in West Turkey, but is also provided to the Levantine Sea by the North African continent, both by Scirocco winds and the Nile (Fig. 4).

In contrast, SL123 in the southern Aegean Sea likely bears a direct impact of Saharan dust. Palygorskite, which is a very good tracer for aeolian dust of North African origin (e.g., Foucault and Mélières, 2000), was identified, but could not be quantified because of its low concentration. The $^{87}Sr/^{86}Sr$ and $^{143}Nd/^{144}Nd$ data also indicate a contribution of Saharan dust (Fig. 7).

Because there is no correlation between smectite/illite ratios indicating the influence of the Nile and the kaolinite/chlorite ratios, we assume that the kaolinite signal is dominated by dust and that it records changes in North African aridity and wind strength. The kaolinite/chlorite ratio shows a long-lasting decreasing trend between 42 ka and ca. 10 ka. This trend clearly results from a decrease in kaolinite concentrations, while chlorite concentrations remain constant (Fig. 3). This finding appears in conflict with the available palaeoclimate data of the region. Atmospheric circulation models consistently indicate an intensification and southward shift of the westerlies during glacial conditions (e.g., Lautenschlager and Herterich, 1990; Joussaume, 1993). This likely resulted in a higher average wind stress and more frequent storms in the eastern Mediterranean region transporting dust from northern Africa into the Eastern Mediterranean Sea. However, the decreasing trend during the late glacial cannot be explained by changing wind strength. More likely, it is a result of decreasing availability. The wind picks up its load in the Saharan desert. Fine-grained sediment

components such as clay occur mainly in areas that were covered by lakes and soils during previous humid periods. In the course of the arid glacial period these source areas became smaller and smaller and thus, less kaolinite was transported by wind.

Alternatively, some of the southern Aegean kaolinite may have also been derived from Nile suspended material and subsequently transported with the eastern Mediterranean surface currents to site SL123 (Fig. 4). At present, kaolinite concentrations of Nile suspended matter are approximately 30% (Stanley and Wingerath, 1996), but during semi-arid conditions of MIS 3 various Egyptian wadi systems may have provided considerably higher amounts of kaolinite. In contrast, during arid conditions of the LGM the fluvial kaolinite flux was likely at a minimum.

The kaolinite/chlorite ratio had minimum values during the African Humid Period and the time of sapropel formation, some 10–6 ka ago (Figs. 4 and 5). During that time the Sahara carried a vegetation cover and therefore erosion was largely reduced (Street and Grove, 1976; Spaulding, 1991; Kutzbach et al., 1996). After that period the kaolinite/chlorite ratios increased stepwise and even reached higher values than during the LGM. This may be due to the fact that after the African Humid Period again large areas of lake sediments and soils were prone to wind erosion. The Sr and Nd isotope signature of late Holocene sediments of SL123 support

our palaeoenvironmental interpretation. The measured $^{87}Sr/^{86}Sr$ and $^{143}Nd/^{144}Nd$ values are characteristic for South Aegean sediments (Weldeab et al., 2002), but exhibit trends consistent with a late Holocene weakening of the Nile influence and strengthening of aeolian sediment input from the Sahara (Figs. 7 and 8).

6.2. Impact of short-term climate variability

In both sediment cores, short-term fluctuations superimpose the long-term trends of grain size distribution and clay mineral composition (Figs. 9 and 10). They are likely linked to climate variations on the northern and southern Mediterranean borderlands. Multi-centennial-to millennial climate changes previously have been reported from different Arctic, Mediterranean and African environments. Greenland ice cores revealed climate variability on millennial timescales with rapid transitions between cold stadials and warm Dansgaard–Oeschger interstadials during the last glacial period (Dansgaard et al., 1993). Spectral analysis showed that these abrupt climate changes occurred at a pacing of 1.470 ka (Grootes and Stuiver, 1997). Recent studies demonstrated that periodic climate changes, though of lower amplitude, also occurred during the Holocene. Thus, North Atlantic drift-ice proxies revealed a 1.470 ± 0.500 ka cycle of cold events (Bond et al., 2001), and spectral analysis of
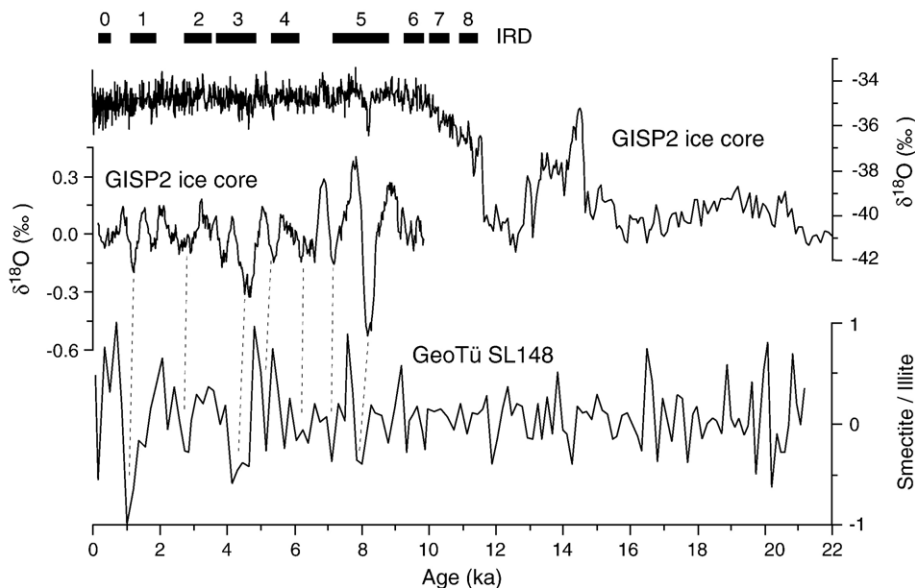

Fig. 9. Correlation of the detrended and normalized smectite/illite ratio of core GeoTü SL148 from the northern Aegean Sea with the $\delta^{18}O$ record of the GISP2 ice core (Grootes et al., 1993) and the smoothed $\delta^{18}O$ time series (300-year running mean) of this ice core for the Holocene section (Schulz and Paul, 2002). Black bars on the upper left indicate Holocene intervals of ice-rafted debris (IRD) in the North Atlantic Ocean (Bond et al., 2001). Holocene cold intervals in the North Atlantic correlate with cool and dry intervals in the northern borderlands of the Eastern Mediterranean.
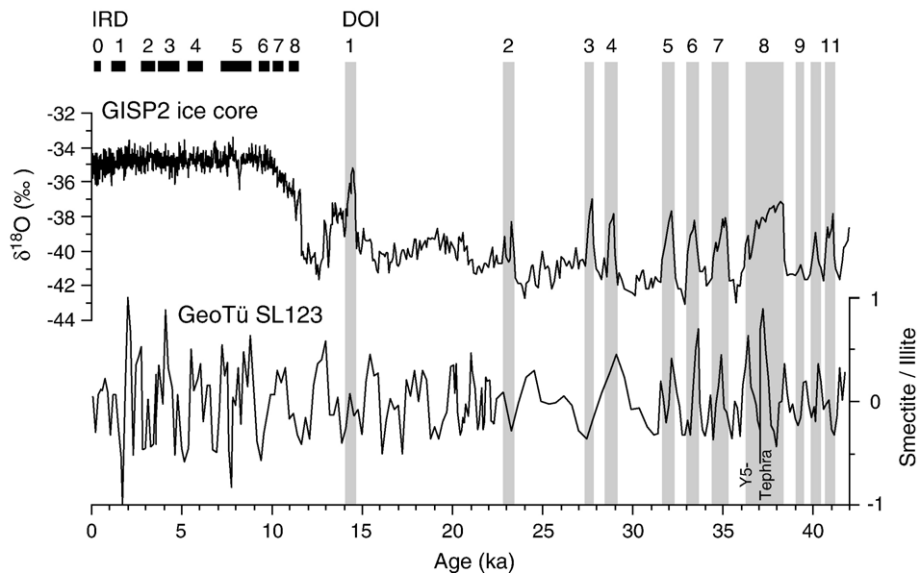
Fig. 10. Correlation of the detrended and normalized smectite/illite ratios of core GeoTü SL123 from the southern Aegean Sea with the $\delta^{18}O$ record of the GISP2 ice core (Grootes et al., 1993). Grey bars indicate Dansgaard–Oeschger Interstadials (DOI). Black bars on the upper left indicate Holocene intervals of ice-rafted debris (IRD) in the North Atlantic Ocean (Bond et al., 2001).

the Holocene section of the GISP ice core record revealed a 900 year cycle of cold events (Schulz and Paul, 2002). In the Aegean Sea, cycles of around 2.300 ka duration occur in proxies of Aegean Sea surface temperature and are correlated to changes of winter/spring intensity of the Siberian High (GISP2 K+ record) and to worldwide Holocene glacier advance phases (Rohling et al., 2002). These observations suggest a significant influence of northern high latitude climate variability on climate and ecosystem variability of the eastern Mediterranean region. Based on the compilation of numerous palynological records, Davis et al. (2003) reconstructed significant vegetation changes in southeastern Europe demonstrating that also the terrestrial ecosystems of this area were very susceptible to marked climate changes during the Holocene.

In the North Aegean Sea core SL148, spectral analysis of the different time series yields high spectral power centred at periods of 1.3–1.8 ka, and subordinately also at 0.85–1.0 ka and 0.7–0.75 ka (Fig. 11). In the detrended smectite/illite ratio these fluctuations are particularly expressed during the Holocene and show a good correlation with the GISP2 ice core (Fig. 9). The minima in smectite/illite correlate with low temperatures in Greenland. In the non-detrended data the smectite/illite ratio exhibits two very prominent incursions with strongly reduced values (Fig. 5). The first one started at 4.9 ka and was centred at 4.4 ka. The second one started at 1.7 ka and was centred at 1.3 ka. Climatic events

occurring at those times are widespread on our globe; however, they are highly variable in their distributions, signs and intensities (Mayewski et al., 2004). In the Greenland ice, cold phases are documented around 5–4 ka and 1.5–1 ka (Schulz and Paul, 2002; Schulz et al., 2004). With an active North Atlantic Oscillation, cold phases in Greenland correspond to dry phases in the Mediterranean region (Cullen et al., 2002).

At around the time of the first event (4.4 ka), the influx of Black Sea Water into the Marmara Sea and Aegean Sea decreased (Fig. 5; Sperling et al., 2003). A 4.2 ka low-latitude drought is documented in many regions of the Eastern Mediterranean, the Near and Middle East and the Arabian Sea (Dalfes et al., 1997). For example, evidence is reported from Italy, Israel, Mesopotamia, northern Africa (Bar-Matthews et al., 1997; Gasse, 2000; Mayewski et al., 2004; Drysdale et al., 2006). Thus, the drastically decreasing smectite/illite ratios in the northern Aegean Sea can be explained by a combination of less smectite formation due to the dry climate and less delivery due to a reduced influx of Black Sea Water. The event coincides with the collapse of the Akkadian empire in Mesopotamia (Weiss et al., 1993; Cullen et al., 2000; deMenocal, 2001) and the Old Kingdom in Egypt (Hassan, 1997). It is not yet understood, why this event finds no expression in the smectite/illite record of the southern core SL123. Between the two events, at ca. 4–2 ka, the smectite/illite ratios do not recapture their former high level (Fig. 5), because the influx of Black Sea Water was generally lower than at 6 ka. The second
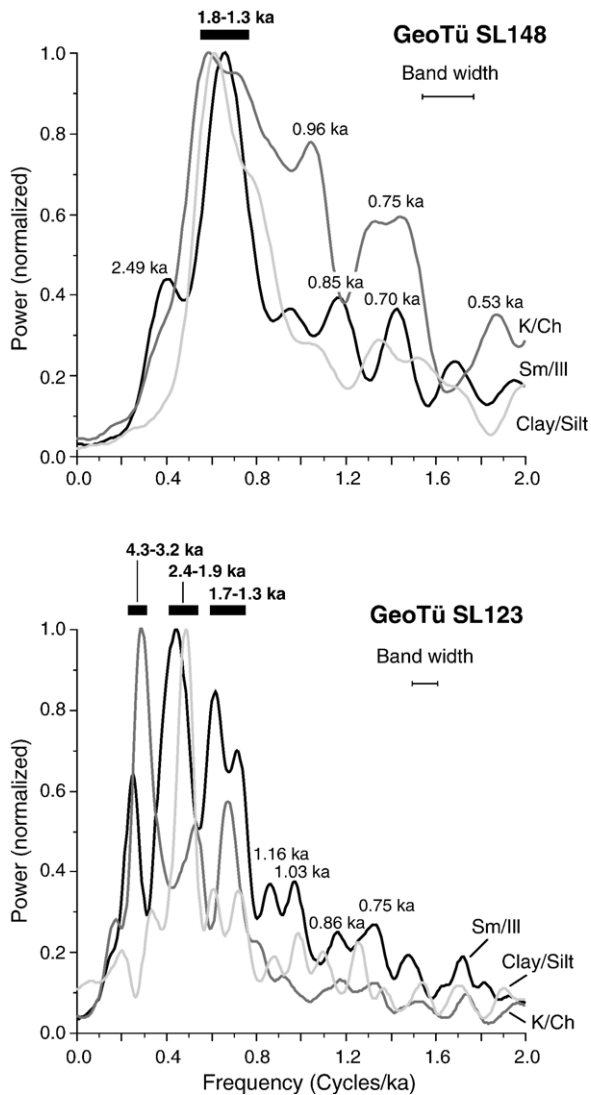
Fig. 11. Blackman–Tukey power spectra of the detrended and normalized smectite/illite (Sm/Ill) ratio, kaolinite/chlorite (K/Ch) ratio, and the clay/silt ratio of cores GeoTü SL148 and SL123 from the North and South Aegean Sea, respectively. The different time series reveal periodic multi-centennial-to millennial variations.

event occurs between the climatic optimum of Roman times and the Medieval Warm Period. Also this period is well known for dry and somewhat cooler conditions (Schulz et al., 2004). After this event, the smectite/illite ratios reach present-day values.

In the southern Aegean Sea periodic short-term variations in the smectite/illite ratio superimpose the long-term trend, both in the Pleistocene and the Holocene. They are centred at various periodicities between 3.2–4.3 ka, 1.9–2.4 ka and 1.3–1.7 ka (Fig. 11). These changes likely mirror fluctuations in

climate of the southern borderlands, especially changes in North African hydrology and Nile discharge. Multi-centennial-to millennial-scale changes in the African monsoon system have been documented in East African lake sediments (Russell and Johnson, 2005), and the Kilimanjaro ice record (Thompson et al., 2002). It is interesting to note that arid intervals are documented in lake sediments in the Mediterranean zone of the Middle Atlas in Morocco that range 7.9–7.5 ka, 5.0–4.9 ka, 3.0–2.8 ka, 1.9–1.7 ka and have similar duration, periodicity and possibly timing to those in the tropics (Fig. 8; Lamb et al., 1995). These dry intervals correlate with periods of low smectite/illite ratios that indicate reduced influence of the Nile. The clay mineral signature at site SL123 implies the absence of significant changes in the surface circulation regime. Comparable periodicities are widely observed in proxy records from the northern hemisphere, suggesting a significant imprint of high-latitude climate variability on North African environments. In this context, the observed 1.3–1.7 ka period is likely equivalent to the pacing of Dansgaard–Oeschger cycles (e.g., Schulz, 2002) (Fig. 10). In the Mediterranean Sea, similar changes have been reported from the western Mediterranean Sea (Cacho et al., 2002) and from eastern Mediterranean terrestrial ecosystems (Allen et al., 1999). To date, no comprehensive data exist from marine records of the eastern Mediterranean Sea. The 1.9–2.4 ka period suggests a relation to solar forcing (Bond et al., 2001) and has been previously recorded in planktic foraminiferal records from the Aegean Sea (Rohling et al., 2002). However, the smectite/illite ratio of core SL123 does not significantly correlate with the planktic record of Rohling et al. (2002) preventing a further evaluation of the underlying mechanisms.

The Holocene fluctuations of the smectite/illite and kaolinite/chorite ratios document the stepwise aridification and desert expansion of Northern Africa and the decrease of East African monsoonal rain fall after the end of the African Humid Period (Fig. 8). The inferred environmental changes are generally consistent with the Nd signature of lithogenic sediment fraction at site SL123 that matches the stepwise decrease of the influence of Nile suspended matter (Fig. 8).

7. Conclusions

The late Quaternary clay fraction of the sediments in the northern and southern Aegean Sea reveal significantly different patterns suggesting that the studied sites were influenced by different source areas, oceanography and climate regimes.

(1) The sea level was the main control for the sedimentation pattern in the northern Aegean Sea. Major sediment fining occurred at ca. 19 ka, 14 ka and 11.3 ka, i.e. directly after the LGM and contemporaneous with meltwater pulses 1A and 1B. The large north Aegean shelf areas submerged with the rising sea level and acted as sediment traps for coarse-grained terrigenous sediment components. Sea level also controlled the kaolinite/chlorite ratio in the northern Aegean Sea, because northward directed ocean currents probably delivered kaolinite. In the southern Aegean Sea, sea level changes did not influence the sedimentation.

(2) A return to cold, near-glacial conditions occurred during the Younger Dryas. The change in vegetation cover as well as in erosion and transport resulted in a coarsening of the sediments in the northern Aegean Sea. Furthermore, lower smectite/illite ratios in the southern Aegean Sea indicate diminished Nile discharge.

(3) Humid conditions with enhanced rainfall and river runoff characterize the African Humid Period and the time of sapropel S1 formation, some 10–6 ka. As a result, sediments coarsened in both the northern and the southern Aegean Sea. Due to a denser vegetation cover, less kaolinite was fed into the Mediterranean Sea resulting in lower kaolinite/chlorite ratios.

(4) The increase in the smectite/illite ratio in the northern Aegean Sea, which started at ca. 8 ka, can be attributed to the establishment of a connection between the Black Sea and the Aegean Sea and/or an enhanced smectite production as a result of the warmer and more humid conditions. The outflow of Black Sea Water into the Aegean Sea changed the oceanographic regime in the northern Aegean Sea towards present conditions, and therefore, also may have influenced sedimentation.

(5) The smectite/illite ratios in the southern Aegean Sea mainly reflect changes in the Nile discharge. Low values characterize the cold and dry climate during the late Pleistocene period, with a minimum during the late glacial. The beginning of humid conditions at ca. 14.5 ka caused an increase in smectite/illite ratios. The most dramatic increase occurred at ca. 9 ka, shortly after the onset of the African Humid Period.

(6) The kaolinite/chlorite ratios in the southern Aegean Sea reflect changes in influx of Saharan dust and therefore in African aridity, wind strength and availability. Especially, the long-

lasting decreasing trend between 42 and 10 ka results from the decreasing availability of fine-grained sediment particles in the source area.

(7) The smectite/illite record in the northern Aegean Sea shows two distinct incursions centred at 4.4 ka and 1.3 ka. The first one corresponds to a well known drought in the regions of the Arabian Sea and the Mediterranean Sea, the second one occurs between the climatic optimum of Roman times and the Medieval Warm Period.

(8) In both sediment cores, short-term fluctuations superimpose the long-term trends of grain size and clay mineral composition. They are probably linked to climate variations on the northern and southern Mediterranean borderlands. In the north, the periodicities are centred at 1.3–1.8 ka, in the south at 3.2–4.3 ka, 1.9–2.4 ka and 1.3–1.7 ka.

Acknowledgements

References

Adamson, D.A., Gasse, F., Street, F.A., Williams, M.A.J., 1980. Late Quaternary history of the Nile. Nature 288, 50–55.

Aksu, A.E., Yasar, D., Mudie, P.J., 1995. Origin of glacial-Holocene hemipelagic sediments in the Aegean Sea: clay mineralogy and carbonate cementation. Mar. Geol. 123, 33–59.

Aksu, A.E., Abrajano, T., Mudie, P.J., Yasar, D., 1999. Organic geochemical and palynological evidence for terrigenous origin of the organic matter in Aegean sapropel S1. Mar. Geol. 153, 303–318.

Allen, J.R.M., Brandt, U., Brauer, A., Hubberten, H.-W., Huntley, B., Keller, J., Kraml, M., Mackensen, A., Mingram, J., Negendank, J.F.W., Nowaczyk, N.R., Oberhänsli, H., Watts, W.A., Wulf, S., Zolitschka, B., 1999. Rapid environmental changes in southern Europe during the last glacial period. Nature 400, 740–742.

Ballard, R.D., Coleman, D.F., Rosenberg, G.D., 2001. Further evidence of abrupt Holocene drowning of the Black sea shelf. Mar. Geol. 170, 253–261.

Balopoulos, E.T., Theocharis, A., Kontoyiannis, H., Varnavas, S., Voutsinou-Taliadouri, F., Iona, A., Souvermezoglou, A., Ignatiades, L., Gotsis-Skretas, O., Pavlidou, A., 1999. Major advances

in the oceanography of the southern Aegean Sea — Cretan Straits system (eastern Mediterranean). Prog. Oceanogr. 44, 109–130.

Bard, E., Hamelin, B., Fairbanks, R.G., Zindler, A., 1990. Calibration of the ^{14}C time scale over the last 30,000 years using mass spectrometric U-Th ages from Barbados corals. Nature 345, 405–410.

Bar-Matthews, M., Ayalon, A., Kaufman, A., 1997. Late Quaternary paleoclimate in the Eastern Mediterranean region from stable isotope analysis of speleothems at Soreq Cave, Israel. Quat. Res. 47, 155–168.

Bar-Matthews, M., Ayalon, A., Kaufman, A., Wasserburg, G.J., 1999. The Eastern Mediterranean paleoclimate as a reflection of regional events: Soreq cave, Israel. Earth Planet. Sci. Lett. 166, 85–95.

Bayhan, E., Ergin, M., Temel, A., Keskin, S., 2001. Sedimentology and mineralogy of surficial bottom deposits from the Aegean–Canakkale–Marmara transition (Eastern Mediterranean): effects of marine and terrestrial factors. Mar. Geol. 175, 297–315.

Biscaye, P.E., 1964. Distinction between kaolinite and chlorite in recent sediments by X-ray diffraction. Am. Mineral. 49, 1281–1289.

Biscaye, P.E., 1965. Mineralogy and sedimentation of recent deep sea clay in the Atlantic Ocean and adjacent seas and oceans. Geol. Soc. Amer. Bull. 76, 803–832.

Bolle, H.-J., 2003. Mediterranean Climate. Regional Climate Studies. Springer, Berlin. 372 pp.

Bond, G., Kromer, B., Beer, J., Muscheler, R., Evans, M.N., Showers, W., Hoddmann, S., Lotti-Bond, R., Hajdas, I., Bonani, G., 2001. Persistent solar influence on North Atlantic climate during the Holocene. Science 294, 2130–2136.

Bottema, S., 1995. The Younger Dryas in the Eastern Mediterranean. Quat. Sci. Rev. 14 (9), 883–891.

Brindley, G.W., Brown, G., 1980. Crystal structures of clay minerals and their X-Ray identification. Miner. Soc. Monogr., vol. 5. 495 pp.

Cacho, I., Grimalt, J.O., Canals, M., Sbaffi, L., Shackleton, N.J., Schönfeld, J., Zahn, R., 2001. Variability of the western Mediterranean Sea surface temperature during the last 25,000 years and its connection with the Northern Hemisphere climatic changes. Paleoceanography 16 (1), 40–52.

Cacho, I., Grimalt, J.O., Canals, M., 2002. Response of the Western Mediterranean Sea to rapid climatic variability during the last 50,000 years: a molecular biomarker approach. J. Mar. Syst. 33–34, 253–272.

Casford, J.S.L., Rohling, E.J., Abu-Zied, R., Coole, S., Fontanier, C., Leng, M., Lykousis, V., 2002. Circulation changes and nutrient concentrations in the late Quaternary Aegean Sea: a nonsteady state concept for sapropel formation. Paleoceanography 17 (2). doi:10.1029/2000PA000601.

Casford, J.S.L., Rohling, E.J., Abu-Zied, R.H., Jorissen, F.J., Leng, M., Schmiedl, G., Thomson, J., 2003. A dynamic concept for eastern Mediterranean circulation and oxygenation during sapropel formation. Palaeogeogr. Palaeoclimatol. Palaeoecol. 190, 103–119.

Chamley, H., 1989. Clay Sedimentology. Springer, Berlin. 623 pp.

Chester, R., Baxter, G.G., Behairy, A.K.A., Connor, K.A., Cross, D., Elderfield, H., Padgham, R.C., 1977. Soil-sized eolian dusts from the lower troposphere of the Eastern Mediterranean Sea. Mar. Geol. 24, 201–217.

COHMAP Members, 1988. Climatic changes of the last 18,000 years: observations and model simulations. Science 241, 1043–1052.

Cramp, A., Collins, M., West, R., 1988. Late Pleistocene — Holocene sedimentation in the NW Aegean Sea: a palaeoclimatic palaeoceanographic reconstruction. Palaeogeogr. Palaeoclimatol. Palaeoecol. 68, 61–77.

Cramp, A., O'Sullivan, G., 1999. Neogene sapropels in the Mediterranean: a review. Mar. Geol. 153, 11–28.

Cullen, H.M., deMenocal, P.B., Hemming, S., Hemming, G., Brown, F.H., Guilderson, T., Sirokko, F., 2000. Climate change and the collapse of the Akkadian empire: evidence from the deep sea. Geology 28 (4), 379–382.

Cullen, H.M., Kaplan, A., Arkin, P.A., deMenocal, P.B., 2002. Impact of the North Atlantic oscillation on Middle Eastern climate and streamflow. Clim. Change 55, 315–338.

Dalfes, H.N., Kukla, G., Weiss, H. (Eds.), 1997. Third Millennium BC Climate Change and Old World Collapse. NATO ASI Series, Series I: Global Environmental Change, vol. 49. Springer, Berlin, Heidelberg. 728 pp.

Davis, B.A.S., Brewer, S., Stevenson, A.C., Guiot, J., 2003. The temperature of Europe during the Holocene reconstructed from pollen data. Quat. Sci. Rev. 22, 1701–1716.

Dansgaard, W., Johnsen, S.J., Clausen, H.B., Dahl-Jensen, D., Gundestrup, N.S., Hammer, C.U., Hvidberg, C.S., Steffensen, J.P., Sveinbjörnsdorf, A.E., Jouzel, J., Bond, G., 1993. Evidence for general instability of past climate from a 250-kyr ice core record. Nature 364, 218–220.

Deino, A.L., Southon, I., Terrasi, F., Campajola, L., Orsi, G., 1994. [14]C and [40]Ar/[39]Ar dating of the Campanian Ignimbrite, Phlegrean Fields, Italy. Abstract ICOG. Berkeley, USA.

deMenocal, P.B., 2001. Cultural response to climate change during the late Holocene. Science 292, 667–672.

deMenocal, P., Ortiz, J., Guilderson, T., Adkins, J., Sarnthein, M., Baker, L., Yarusinsky, M., 2000. Abrupt onset and termination of the African Humid Period: rapid climate responses to gradual insolation forcing. Quat. Sci. Rev. 19, 347–361.

Druitt, T.H., Edwards, L., Mellors, R.M., Pyle, D.M., Sparks, R.S.J., Lanphere, M., Davies, M., Barriero, B., 1999. Santorini Volcano. Geol. Soc. Spec. Publ, vol. 19. 165 pp.

Drysdale, R., Zanchetta, G., Hellstrom, J., Maas, R., Fallick, A., Pickett, M., Cartwright, I., Piccini, L., 2006. Late Holocene drought responsible for the collapse of Old World civilizations is recorded in an Italian cave flowstone. Geology 34 (2), 101–104.

Ehrmann, W., Schmiedl, G., Hamann, Y., Kuhnt, T., in press. Distribution of clay minerals in surface sediments of the Aegean Sea: A compilation. Int. J. Earth Sci. (Geol. Rdsch.). doi:10.1007/s00531-006-0119-1.

Emeis, K.-C., Sakamoto, T., Wehausen, R., Brumsack, H.-J., 2000. The sapropel record of the eastern Mediterranean Sea — results of Ocean Drilling Program Leg 160. Palaeogeogr. Palaeoclimatol. Palaeoecol. 158, 371–395.

Esquevin, J., 1969. Influence de la composition chimique des illites sur le cristallinité. Bull. Cent. Rech. Pau S.N.P.A. 3, 147–154.

Fairbanks, G., Mortlockyr, R.A., Chiua, T.-C., Caoa, L., Kyrplana, A., Guildersonc, T.P., Fairbanks, T.W., Bloom, A.L., Grootes, P.M., Nadeau, M.-J., 2005. Radiocarbon calibration curve spanning 0 to 50,000 years BP based on paired [230]Th/[234]U and ^{14}C dates on pristine corals. Quat. Sci. Rev. 24, 1781–1796.

Felis, T., Lohmann, G., Kuhnert, H., Lorenz, S.J., Scholz, D., Pätzold, J., Al-Rousan, S., Al-Moghrabi, S., 2004. Increased seasonality in Middle East temperatures during the last interglacial period. Nature 429, 164–168.

Foucault, A., Mélières, F., 2000. Palaeoclimatic cyclicity in central Mediterranean Pliocene sediments: the mineralogical signal. Palaeogeogr. Palaeoclimatol. Palaeoecol. 158, 311–323.

Frumkin, A., Stein, M., 2004. The Sahara — East Mediterranean dust and climate connection revealed by strontium and uranium

isotopes in a Jerusalem speleothem. Earth Planet. Sci. Lett. 217, 451–464.

Gasse, F., 2000. Hydrological changes in the African tropics since the Last Glacial Maximum. Quat. Sci. Rev. 19, 189–211.

Geraga, M., Tsaila-Monopolis, S., Joakim, C., Papatheodorou, G., Ferentinos, G., 2000. Evaluation of palaeoenvironmental changes during the last 18,000 years in the Myrtoon basin, SW Aegean Sea. Palaeogeogr. Palaeoclimatol. Palaeoecol. 156, 1–17.

Geraga, M., Tsaila-Monopolis, S., Ioakim, C., Papatheodorou, G., Ferentinos, G., 2005. Short-term climate changes in the southern Aegean Sea over the last 48,000 years. Palaeogeogr. Palaeoclimatol. Palaeoecol. 220, 311–332.

Griffin, J.J., Windom, H., Goldberg, E.D., 1968. The distribution of clay minerals in the World Ocean. Deep-Sea Res. 15, 433–459.

Grootes, P.M., Stuiver, M., 1997. Oxygen 18/16 variability in Greenland snow and ice with 10^{-3} to 10^5 year time resolution. J. Geophys. Res. C102, 26455–26470.

Grootes, P.M., Stuiver, M., White, J.W.C., Johnson, S., Jouzel, J., 1993. Comparison of oxygen isotope records from GISP2 and GRIP Greenland ice cores. Nature 366, 552–554.

Gupta, A.K., Das, M., Anderson, D.M., 2005. Solar influence on the Indian summer monsoon during the Holocene. Geophys. Res. Lett. 32, L17703. doi:10.1029/2005GL022685.

Hammer, C.U., Clausen, H.B., Friedrich, W.L., Tauber, H., 1987. The Minoan eruption of Santorini in Greece dated to 1645 BC? Nature 328, 517–519.

Hassan, F.A., 1997. Holocene paleoclimate of Africa. Afr. Archaeol. Rev. 14 (4), 213–230.

Hoogakker, B.A.A., Rothwell, R.G., Rohling, E.J., Paterne, M., Stow, D.A.V., Herrle, J.O., Clayton, T., 2004. Variations in terrigenous dilution in western Mediterranean Sea pelagic sediments in response to climate change during the last glacial cycle. Mar. Geol. 211, 21–43.

Jacobson, S.B., Wasserburg, G.J., 1980. Sm-Nd isotopic evolution of chondrites. Earth Planet. Sci. Lett. 50, 139–155.

Jorisson, F.J., Asioli, A., Borsetti, A.M., Capotondi, L., de Visser, J.P., Hilgen, F.J., Rohling, E.J., van der Borg, K., Vergnaud Grazzini, C., Zachariasse, W.J., 1993. Late Quaternary central Mediterranean biochronology. Mar. Micropaleontol. 21, 169–189.

Joussaume, S., 1993. Paleoclimatic tracers: an investigation using an atmospheric general circulation model under ice age conditions. J. Geophys. Res. 98, 2767–2805.

Karageorgis, A.P., Kaberi, H.G., Tengberg, A., Zervakis, V., Hall, P.O.J., Anagnostou, C., 2003. Comparison of particulate matter distribution, in relation to hydrography, in the mesotrophic Skagerrak and the oligotrophic northeastern Aegean Sea. Cont. Shelf Res. 23, 1787–1809.

Karageorgis, A.P., Anagnostou, C.L., Kaberi, H., 2005. Geochemistry and mineralogy of the NW Aegean Sea surface sediments: implications for river runoff and anthropogenic impact. Appl. Geochem. 20, 69–88.

Kubilay, N.N., Sydam, A.C., Yemenicioglu, S., Kelling, G., Kapur, S., Karaman, C., Akça, E., 1997. Seasonal chemical and mineralogical variability of atmospheric particles in the coastal region of the Northeastern Mediterranean. Catena 28, 313–328.

Kutzbach, J., Bonan, G., Foley, J., Harrison, S.P., 1996. Vegetation and soil feedbacks on the response of the African monsoon to orbital forcing in the early to middle Holocene. Nature 384, 623–626.

Krom, M.D., Cliff, R.A., Eijsink, L.M., Herut, B., Chester, R., 1999. The characterisation of Saharan dusts and Nile particulate matter in surface sediments from the Levantine basin using Sr isotopes. Mar. Geol. 155, 319–330.

Krom, M.D., Stanley, J.D., Cliff, R.A., Woodward, J.C., 2002. Nile River sediment fluctuations over the past 7000 years and their key role in sapropel development. Geology 30 (1), 71–74.

Lamb, H.F., Gasse, F., Benkaddour, A., El Hamouti, N., Van der Kaars, S., Perkins, W.T., Perarce, N.J., Roberts, C.N., 1995. Relation between century-scale Holocene arid intervals in tropical and temperate zones. Nature 373, 134–137.

Lautenschlager, M., Herterich, K., 1990. Atmospheric response to ice age conditions: climatology near the Earth's surface. J. Geophys. Res. 95, 22,547–22,557.

Lykousis, V., Chronis, G., Tselepides, A., Price, N.B., Theocharis, A., Siokou-Frangou, I., Van Wambeke, F., Danovaro, R., Stavrakakis, S., Duineveld, G., Georgopoulos, D., Ignatiades, L., Souvermezoglou, A., Voutsinou-Talidouri, F., 2002. Major outputs of the recent multidisciplinary biogeochemical researches undertaken in the Aegean Sea. J. Mar. Syst. 33–34, 313–334.

Martrat, B., Grimalt, J.O., Lopez-Martinez, C., Cacho, I., Sierro, F.J., Flores, J.A., Zahn, R., Canals, M., Curtis, J.H., Hodell, D.A., 2004. Abrupt temperature changes in the western Mediterranean over the past 250,000 years. Science 306, 1762–1765.

Mayewski, P.A., Rohling, E.E., Stager, J.C., Karlen, W., Maasch, K.A., Meeker, L.D., Meyerson, E.A., Gasse, F., Van Kreveld, S., Holmgren, K., Lee-Thorp, J., Rosqvist, G., Rack, F., Staubwasser, M., Schneider, R.R., Steig, E.J., 2004. Holocene climate variability. Quat. Res. 62, 243–255.

Meyers, P.A., 2006. Paleoceanographic and paleoclimatic similarities between Mediterranean sapropels and Cretaceous black shales. Palaeogeogr. Palaeoclimatol. Palaeoecol. 235, 305–320.

Minoura, K., Imamura, F., Kuran, U., Nakamura, T., Papadopoulos, G.A., Takahashi, T., Yalciner, A.C., 2000. Discovery of Minoan tsunami deposits. Geology 28, 59–62.

Myers, P.G., Haines, K., Rohling, E.J., 1998. Modeling the paleocirculation of the Mediterranean: the last glacial maximum and the Holocene with emphasis on the formation of sapropel S1. Paleoceanography 13 (6), 586–606.

Mommersteeg, H.J.P.M., Loutre, M.F., Young, R., Wijmstra, T.A., Hooghiemstra, H., 1995. Orbital forced frequencies in the 975000 year pollen record from Tenaghi Philippon (Greece). Clim. Dyn. 11, 4–24.

Paillard, D., Labeyrie, L., Yiou, P., 1996. Macintosh program performs time series analysis. EOS 77, 379.

Perissoratis, C., Conispoliatis, N., 2003. The impacts of sea level changes during the latest Pleistocene and Holocene times on the morphology of the Ionian and Aegean seas (SE Alpine Europe). Mar. Geol. 196, 145–156.

Petschick, R., Kuhn, G., Gingele, F., 1996. Clay mineral distribution in surface sediments of the South Atlantic: sources, transport, and relation to oceanography. Mar. Geol. 130, 203–229.

Pickard, G.L., Emery, W.J., 1990. Descriptive Physical Oceanography. Pergamon Press. 320 pp.

Pinardi, N., Masetti, E., 2000. Variability of the large scale general circulation of the Mediterranean Sea from observations and modelling: a review. Palaeogeogr. Palaeoclimatol. Palaeoecol. 158, 153–173.

Poulos, S.E., Collins, M.B., Shaw, H.F., 1996. Deltaic sedimentation, including clay mineral deposition patterns, associated with small mountainous rivers and shallow marine embayments of Greece (SE Alpine Europe). J. Coast. Res. 12, 940–952.

Pye, K., 1992. Aeolian dust transport and deposition over Crete and adjacent parts of the Mediterranean Sea. Earth Surf. Process. Landf. 17, 271–288.

Rohling, E.J., 1994. Review and new aspects concerning the formation of eastern Mediterranean sapropels. Mar. Geol. 122, 1–28.

Rohling, E.J., Hilgen, F.J., 1991. The eastern Mediterranean climate at times of sapropel formation: a review. Geol. Mijnb. 70, 253–264.

Rohling, E., Pählike, H., 2005. Centennial-scale climate cooling with a sudden cold event around 8,200 years ago. Nature 434, 975–979.

Rohling, E.J., Mayewski, P.A., Ramadan, H.A., Casford, J.S.L., Hayes, A., 2002. Holocene atmosphere-ocean interactions; records from Greenland and the Aegean Sea. Clim. Dyn. 18, 587–593.

Rossignol-Strick, M., 1983. African monsoons, an immediate climate response to orbital insolation. Nature 304, 46–49.

Rossignol-Strick, M., Nesteroff, W., Olive, P., Vergnaud-Grazzini, C., 1982. After the deluge: Mediterranean stagnation and sapropel formation. Nature 295, 105–110.

Russell, J.M., Johnson, T.C., 2005. A high-resolution geochemical record from Lake Edward, Uganda Congo and the timing and causes of tropical African drought during the late Holocene. Quat. Sci. Rev. 24, 1375–1389.

Ryan, W.B.F., Pitman III, W.C., Major, C.O., Shimkus, K., Moskalenko, V., Jones, G.A., Dimitrov, P., Gorur, N., Sakinc, M., Yuce, H., 1997. An abrupt drowning of the Black Sea shelf. Mar. Geol. 138, 119–126.

Schilman, B., Bar-Matthews, M., Almogi-Labin, A., Luz, B., 2001. Global climate instability reflected by Eastern Mediterranean marine records during the late Holocene. Palaeogeogr. Palaeoclimatol. Palaeoecol. 176, 157–176.

Schulz, M., 2002. On the 1470-year pacing of Dansgaard–Oeschger warm events. Paleoceanography 17 (2). doi:10.1029/2000PA000571.

Schulz, M., Paul, A., 2002. Holocene climate variability on centennial-to-millennial time scales: 1. Climate records from the North-Atlantic Realm. In: Wefer, G., Berger, W., Behre, K.-E., Jansen, E. (Eds.), Climate Development and History of the North Atlantic Realm. Springer, Berlin, pp. 41–45.

Schulz, M., Paul, A., Timmermann, A., 2004. Glacial-interglacial contrast in climate variability at centennial-to-millennial time-scales: observations and conceptual model. Quat. Sci. Rev. 23, 2219–2230.

Seymour, K.S., Christanis, K., Bouzinos, A., Papazisimou, S., Papatheodorou, G., Moran, E., Dénès, G., 2004. Tephrostratigraphy and tephrochronology in the Philippi peat basin, Macedonia, Northern Hellas (Greece). Quat. Int. 121, 53–65.

Siani, G., Paterne, M., Michel, E., Sulpizio, R., Sbrana, R., Arnold, M., Haddad, G., 2001. Mediterranean Sea surface radiocarbon reservoir age changes since the Last Glacial Maximum. Science 294, 1917–1920.

Spaulding, W.G., 1991. Pluvial climatic episodes in North America and North Africa: types and correlation with global climate. Palaeogeogr. Palaeoclimatol. Palaeoecol. 84, 217–227.

Sperling, M., Schmiedl, G., Hemleben, Ch., Emeis, K.-C., Erlenkeuser, H., Grootes, P.M., 2003. Black sea impact on the formation of eastern Mediterranean sapropel S1? Evidence from the Marmara Sea. Palaeogeogr. Palaeoclimatol. Palaeoecol. 190, 9–21.

Stanley, D.J., Wingerath, J.G., 1996. Clay mineral distributions to interpret Nile cell provenance and dispersal, I. Lower River Nile to delta sector. J. Coast. Res. 12, 911–929.

Stratford, K., Williams, R.G., Myers, P.G., 2000. Impact of the circulation on sapropel formation in the eastern Mediterranean. Glob. Biogeochem. Cycles 14 (2), 683–695.

Street, F.A., Grove, A.T., 1976. Environmental and climatic implications of late Quaternary lake-level fluctuations in Africa. Nature 261, 385–390.

Talbot, M.R., Williams, M.A.J., Adamson, D.A., 2000. Strontium isotope evidence for late Pleistocene reestablishment of an integrated Nile drainage network. Geology 28, 343–346.

Thompson, L.G., Mosley-Thompson, E., Davis, M.E., Henderson, K.A., Brecher, H.H., Zagorodnov, V.S., Mashiotta, T.A., Lin, P.-N., Mikhalenko, V.N., Hardy, D.R., Beer, J., 2002. Kilimanjaro ice core records: evidence of Holocene climate change in tropical Africa. Science 298, 589–593.

Tomadin, L., Lenaz, R., Landuzzi, V., Mazzucotelli, A., Vannucci, R., 1984. Wind-blown dust over the Central Mediterranean. Oceanol. Acta 7 (1), 13–23.

Venkatarathnam, K., Ryan, W.B.F., 1971. Dispersal patterns of clay minerals in the sediments of the eastern Mediterranean Sea. Mar. Geol. 11, 261–282.

Weaver, C.E., 1989. Clays, muds and shales. Developments in Sedimentology, vol. 44. Elsevier. 819 pp.

Weldeab, S., Emeis, K.-C., Hemleben, C., Siebel, W., 2002. Provenance of lithogenic surface sediments and pathways of riverine suspended mattern in the Eastern Mediterranean Sea: evidence from $^{143}Nd/^{144}Nd$ and $^{87}Sr/^{86}Sr$ ratios. Chem. Geol. 186, 139–149.

Weiss, H., Courty, M.-A., Wetterstrom, W., Guichard, F., Senior, L., Meadow, R., Curnow, A., 1993. The Genesis and collapse of third millennium North Mesopotamian civilization. Science 261, 995–1004.

Windom, H.L., 1976. Lithogenous material in marine sediments. In: Riley, J.P., Chester, R. (Eds.), Chemical Oceanography, vol. 5. Academic Press, New York, pp. 103–135.

Wulf, S., Kraml, M., Kuhn, T., Schwarz, M., Inthorn, M., Keller, J., Kuscu, I., Halbach, P., 2002. Marine tephra from the Cape Riva eruption (22 ka) of Santorini in the Sea of Marmara. Mar. Geol. 183, 131–141.

Wüst, G., 1961. On the vertical circulation of the Mediterranean Sea. J. Geophys. Res. 66, 3261–3271.